Assessment, STrategy And Risk Reduction for Tsunamis in Europe

Project nº 603839, co-financed by the EC (FP7)

Deliverable 2.43

New results of the offshore record

of tsunami deposits and MTDs in the NEAM region:

The southwestern iberian margin case

ABRIL 2017

Assessment, STrategy And Risk Reduction for Tsunamis in Europe

(Project nº 603839, co-financed by the EC (FP7))
PI- Maria Ana Viana Baptista

Deliverable 2.43

New results of the offshore record of tsunami deposits and MTDs in the NEAM region: **the southwestern iberian margin case**.

ABRIL 2017

Contribution of: Pedro Terrinha (1,2), Pedro Noiva (1), Pedro Brito (1,2), Luís Baptista(1,2), Cristina Roque (2,3), Teresa Drago(1,2), Pedro Silva(2,4), Vitor Magalhães (1,2), Ana Isabel Rodrigues (1) & Ana Lopes (1)

(1) Instituto Português do Mar e da Atmosfera (IPMA); (2) Instituto Dom Luiz, Universidade de Lisboa, Portugal; (3)- Estrutura Missão para a Extensão da Plataforma (EMEPC); (4) - Instituto Superior de Engenharia de Lisboa, Instituto Politécnico de Lisboa, Lisboa, Portugal (ISEL)

Contents

I. Results from the study of offshore gravity cores 1
1. INTRODUCTION 1
2- STATE OF ART 2
3. METHODOLOGY 4
3.1. Sedimentological analyses 5
3.2. Multi-sensor Core Logger data 5
3.3. XRF Core Scanner data 5
3.4. Magnetic analyses 6
4. RESULTS 7
4.1. Description 7
4.2. Sedimentology 9
4.3. Magnetism 13
4.4. – Multi-Sensor Core Logger data 22
4.5. X-Ray Fluorescence data 24
4.6. AMS C^{14} and Pb^{210} dating 30
5. DISCUSSION 33
5.1. Searching for evidences of offshore tsunamigenic deposits 33

II. Results from the acquisition and study of offshore seismic reflection seismics 35
1.Introduction 35
2. MTDs from seismic reflection profiles 35
2.1 The Hirondelle seamount 35
2.2 The Tagus delta landslide 38
2.3 The Algarve MTDs 39

III. FINAL CONSIDERATIONS 45
The Algarve coast 45
The Tagus river 45
The South Hirondelle Landslide 45

IV. OUTREACH 45

Acknowledgments 46

References 46

I. Results from the study of offshore gravity cores

1. INTRODUCTION

Tsunamis can cause countless human and economic losses. Therefore, it is important to assess the tsunami hazard in order to prevent and/or minimize its effects. This task is only possible if a complete dataset of events is available, allowing the determination of the recurrence intervals of the tsunamis adapted to local and regional conditions thus giving support to the design of warning systems and mitigation measures.

WP2 of ASTARTE intends to go beyond tsunamis catalogues, incorporating novel geological and geophysical contribution and new statistical analyses for the assessment of the long-term recurrence rates of large events in sensitive areas of the North East Atlantic region. In this context, the objectives of the WP2.2 were focused on the evaluation of tsunami recurrence rates from the continental shelf sedimentary record.

Tsunami onshore evidences are widely recognized all over the world. Contrarily, the knowledge of tsunami and paleo tsunami backwash deposits in continental shelf remains very poorly explored. The investigation of such records is crucial to better understand tsunami spread and consequences, to provide information for a probabilistic estimation of tsunami occurrences and to improve hazard assessment. With this objective, it was foreseen to acquire new cores in the South Portuguese Margin, during a MeBo drill cruise with the RV Merian that was programmed to improve the knowledge about historic and pre-historic tsunamis in this region. However, the MeBo drill cruise was not performed and so, the study was dedicated on some pre-existing cores from the POPEI project (FCT- POCTI/MAR/55618/2004), and one year after on MOWER cores, collected in a Spanish cruise where one of the ASTARTE members was participated. These cores are located in the Faro MTD area where the ASTARTE 2014 high resolution multichannel seismic campaign was acquired to search for and map tsunami deposits and/or erosion structures caused by tsunamis in the continental shelf sedimentary record off Quarteira-Tavira in the Algarve, south Portugal (see chapter 2).

POPEI gravity cores were collected in southern Portuguese continental shelf, westward of Cabo Sta Maria, at depths between 70 and 100m (Figure 1). They were sampled in 2008 and preserved at temperatures of 4ºC. The gravity cores have a length varying between 1.41m and 1.84m (Table I).

MOWER gravity cores were collected in September of 2014 on board the R/V Sarmiento de Gamboa in the context of the Spanish national project with the same name (CTM 2012-39599-C03) (Figure 1). They were obtained at sites located between 56.76 m and 90.81 m, and near POPEI cores. The length of the cores range between 1.25 and 3.53m (Table 1).

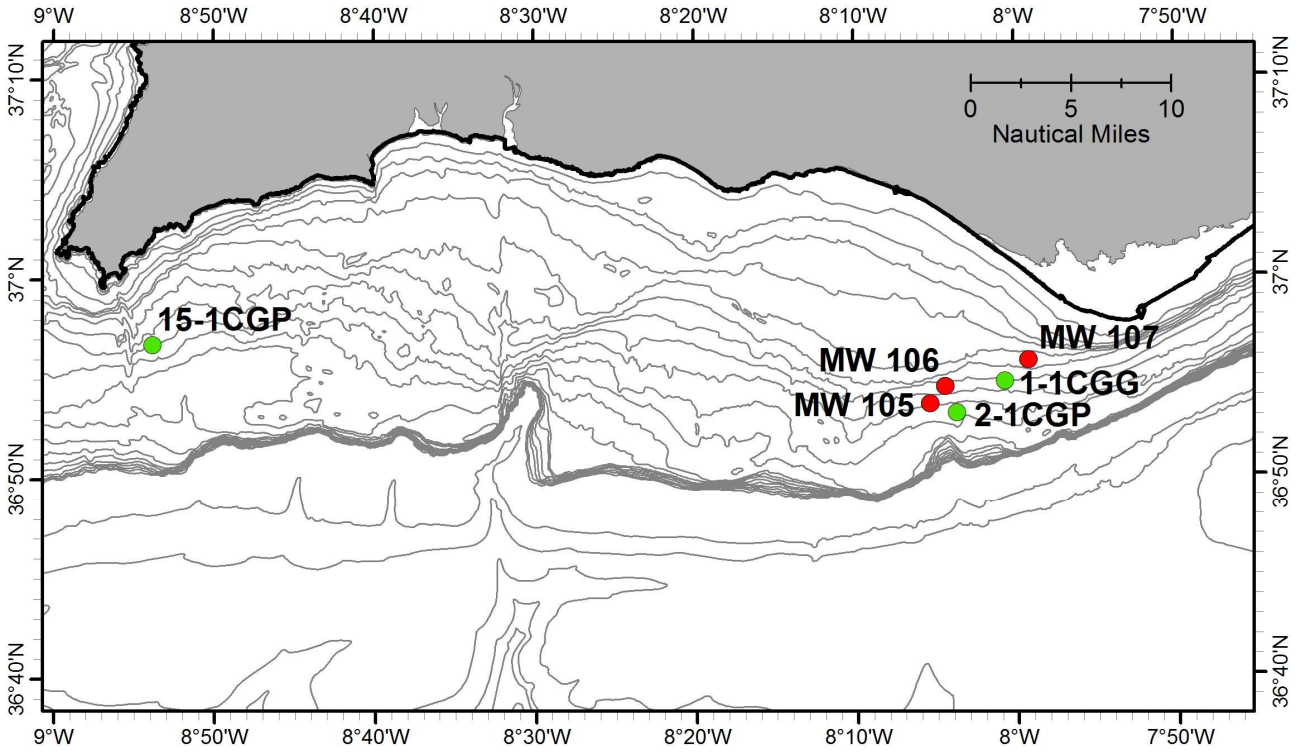

Figure 1 – Location of the POPEI (1-1CGG, 2-1CGP and 15-1CGP) and MOWER (MW105, MW106 and MW107) cores.

Table I – Location, water depth and length of the studied cores.

Name	Coordinates		Water Depth (m)	Length (m)
	Latitude	Longitude		
1- 1CGG	36.9123235 36º 54' 44.36'' N	8.0117995 8º 00' 42.48'' W	76m	1.84m
2-1CGP	36.88595767 - 36º 53' 9.45'' N	-8.061872 -8º 3' 42.74'' W	84.45 m	1.80m
15-1CGP	36.94533383 36º 56' 43.20'' N	-8.897040333 -8º 53' 49.35'' W	87.14 m	1.41m
MW105	36.9079325	-8.073539336	76.11m	2.50m
MW106	36.89356417	-8.073195878	90.81m	3.53m
MW107	36.92940173	-7.986915312	56.76m	1.25m

2- STATE OF ART

The knowledge of past tsunami events are made through instrumental, historical and geological records. Although instrumental and historical records are very important, they are limited in time.

The sedimentary record is a useful tool for obtaining paleoseismic information since it is the only record available that allows us to detect and to analyze ancient offshore seismicity. They provide evidence of past tsunami effects and provide estimates of tsunami recurrence and magnitude, which can be used to improve our understanding of tsunamis and help mitigate the hazards from future tsunamis.

Tsunamis are capable to trigger sediment movement in two generally different ways. When the tsunami wave exceeds a critical current velocity, unconsolidated sediment is eroded. This sediment is transported in suspension and as traction load until the current falls below a critical transport velocity. Sediments that are actively transported by tsunami waves – either landward (onshore deposits) or seaward (offshore deposits) – are called “tsunami deposits” (Dawson and Stewart, 2007). In addition, tsunamis can trigger submarine slides of material at instable slopes that moves downhill in the form of turbidity currents. Both, actively transported deposits and tsunami induced gravity movements are summarized with the term “tsunamiite” (Shiki and Yamazaki, 1996) or “tsunamite” (Shanmugam, 2006).

Common for all of these tsunami-induced deposits are the characteristic properties of “event deposits”, i.e. episodic occurrence and unusually high-energetic transport processes compared to the autochthonous background deposition.

The recognition of palaeotsunami deposits and reconstruction of the generating events depends solely on the interpretation of geological data. The sedimentary recognition of tsunami deposits is based upon a group of textural, lithostratigraphic, palaeontological and geochemical data that has been used by many authors over recent years. This literature is dominated by cases from Japan, Cascadia (northern California to southern British Columbia), and the 2004 Indian Ocean tsunami. Other localities with concentrated studies include New Zealand, the Russian Far East, Alaska, Chile and Peru, the 1929 Grand Banks event, and the 1755 Lisbon earthquake and tsunami. While there are few studies of prehistoric tsunami deposits in low-latitude regions, surveys of recent tsunami effects, In addition to 2004, include Indonesia, Philippines, Papua New Guinea, Hawaii, Peru, Nicaragua, the Caribbean and Mediterranean.

In what concern the Iberian margin, many onshore studies on tsunami deposits have been published since the 1990s and they are essentially focused in sedimentary records located on estuaries, marshes, beach-

barriers (spit-bars), and some coastal lowlands. In Portugal, tsunami deposits have been described in Aveiro (Corrochano *et al*. 2000); Tejo (Andrade *et al*., 2003), Cascais (Scheffers & Kelletat, 2005) and in the southern coast, Algarve (Andrade et al., 1997, Kortekaas & Dawson, 2007; Costa et al., 2011; Dawson et al., 1995, Hindson and Andrade, 1999, Hindson et al., 1996; Costa et al., 2009, Schneider et al., 2009; Andrade, 1992). In the Spanish coast along Golf of Cadiz, several studies were performed: Guadalquivir (Lario et al., 1995, 2001a, b; Lario, 1996; Ruiz et al., 2004, 2005; Cáceres et al., 2006), Tinto-Odiel (Lario, 1996; Ruiz et al., 2007; Morales et al., 2008), Doñana - Ruiz et al. (2005), Guadalete (Lario et al., 1995; Lario, 1996; Dabrio et al., 1999; Luque et al., 2001, 2002) estuaries, the littoral lowland on the south-eastern coast of the Gulf of Cadiz (Luque, 2002; Cap Trafalgar (Whelan and Kelletat, 2005); Gilbratar (Reicherter et al., 2010).

Whereas the onshore effects of tsunamis have received much attention along the coastlines of the world, research focusing on geologic evidences of tsunami transport and deposition in the offshore zones or in shallow-shelf areas are very few, as recognized by Dawson &Stewart (2007). It was the case of the identification of tsunami deposits along the Portuguese coast has been mostly conducted onshore (e.g. Dawson *et al*., 1995; Hindson *et al.*, 1996; Font *et al*., 2010; Costa *et al.*, 2012), but remains scarce on the offshore domains (Abrantes *et al.*, 2005, 2008; Quintela, 2016).

In the case of Iberia margin, and more particularly on the continental shelf offshore Delta Tejo, magnetic susceptibility, grain-size and XRF-Fe data found evidences that both 1969 AD (Abrantes et al., 2008) and the 1755 AD (Abrantes et al., 2005, 2008) earthquake-originated tsunami left a sedimentary imprint in the shallow-shelf environment off Lisbon.

Moreover, although some work suggested the presence of earthquake triggered turbidites in the SW Iberian margin this area (Thomson &Weaver, 1994; Lebreiro et al., 1997) it was only recently that the first paper about turbidite seismology appeared, studying the sediments related to 20th century earthquakes (Garcia-Orellana et al., 2006). Six short sediment cores (50 cm long) were collected by a multicorer in the area stretching from the Tagus to the Horseshoe Abyssal plains for radiometric (210Pb and 137Cs) and sedimentological analyses. Garcia-Orellana et al. (2006) related the turbidites found with the historical and instrumental earthquakes that occurred in the SW Portuguese Margin, namely, the 1909 Benavente and 1969 Horseshoe earthquakes.

Also, Vizcaino et al. (2006) dated and correlated turbidites sampled near active faults and slope basins with those found in the neighboring Horseshoe and Tagus abyssal plains (e.g. Lebreiro et al. 1997) given that synchronous and widely spaced Holocene turbidites are likely to be generated by great earthquakes (Adams, 1990; Goldfinger et al. 2003). However, regardless of the triggering mechanism of the mass wasting deposits around the Marquês de Pombal area, the data presented

in this paper clearly indicate that the large landslide deposits observed on the acoustic backscatter map are not related to the 1755 Lisbon Earthquake, but are much older, with ages between c. 3270 and 1940 yr BP. Surprisingly, the mass wasting event that is a possible candidate for correlation with the 1755 Lisbon earthquake is T1, which is only represented by a thin turbidite in one of the cores.

Later on, Gràcia et al. (2010) made a correlation between synchronous turbidite layers found in long distance apart basins (Tagus Abyssal Plain, Infante Don Henrique Basin and Horseshoe Abyssal Plain). The final result was a turbidite event chronology for the SW Iberian Margin with a total of 14 turbidite events in the last 16.5 ka (E1–E14), of which 11 occurred during the Holocene.

Widespread turbidites deposited during the Holocene suggest that they are related to great earthquakes (Mw_ 8.0) occurred in the SW Iberian Margin. Widespread turbidite events E1 (AD1971_3), E3 (300–560 yr BP) and E5 (1980–2280 yr BP) can be correlated with instrumental and historical earthquakes that occurred during the last 2500 years, such as theAD1969Horseshoe Earthquake, theAD1755LisbonEarthquake and Tsunami, and the 218 BC Earthquake and Tsunami, respectively. Older widespread Holocene events E6 (4960–5510 yr BP) and E8 (6690–6985 yr BP) can be correlated with tsunami deposits that occurred around 5310 yr BP and 6000–7000 yr BP, respectively. On the basis of synchronicity, E10 (8715–9015 yr BP) may also be regarded as a seismically triggered event. In contrast, the fact that E9 occurred immediately after the 8.2 ka climatic event suggests the possibility of a non-seismic origin for its associated turbidite layers. As regards the non-wide spread Holocene turbidites E2 (AD1908_ 8), E4 (855–1110 yr BP) and E7 (6110–6365 yr BP), the first two could be related to low-moderate magnitude historical earthquakes, although no further evidence is available to support this interpretation. In this context, the recurrence interval for great earthquakes determined is approximately 1800 years.

3. METHODOLOGY

Despite the ability of continental shelf sediments in providing more continuous than continental records, the identification of tsunami deposits in marine environments is complex. Sedimentary hiatus promoted by the removal of the superficial layers by tsunami waves, abrupt increase of the terrigenous inputs brought by the backwash waves (e.g. Abrantes *et al.*, 2005, 2008) and diagenesis are some of the mechanical and chemical processes that should be taken into account. Therefore, when searching for tsunamigenic layers we are looking for abrupt changes of the sedimentary regime as for the existence of anomalous magnetic and geochemical signatures in the sedimentary record regarding the existence of allochthonous sediment.

With this purpose, a multi-disciplinary approach including photo, X-ray, Multi Sensor Corer Logger (MSCL) and X-ray Fluorescence (XRF) were performed in Bremen University, for POPEI cores and in University of Vigo for MOWER cores; visual description was made at IPMA-Algés, sedimentological analysis (grain-size, carbonates and organic matter) was mostly performed at IPMA-Tavira geological lab and magnetic (magnetic susceptibility, thermomagnetic analyses, acquisition of magnetizations, natural remnant magnetization and anisotropy of magnetic susceptibility) analysis at Instituto D. Luiz (IDL - Faculty of Sciences in University of Lisbon). These analyses were complemented by AMS C14 dating at Beta Analytic Inc. (USA) and Actalabs (Canada) and by Pb210 at Bordeaux I University (France) (Table II).

In the studied cores, POPEI (1-1CGG, 2-1CGP, 15-1CGP) and MOWER (MW105, MW106 and MW107), a 1cm resolution analysis was made for all the sedimentological, magnetic, physical properties and geochemical analyses.

Table II – The sites and the analysis made to POPEI and MOWER cores. Legend: gs – grain size; c – carbonates, om – organic matter; χ_{LF} – low-field magnetic susceptibility; χ_{FD} frequency dependence of magnetic susceptibility; ARM Anhysteretic remanent magnetization, IRM – isothermal remanent magnetization, NRM – natural remanent magnetization; AMS – Anisotropy of magnetic susceptibility.

Project	**Cores**	**Visual description** IPMA Algés	**Sedimentology** Ipma (Tavira+Algés)	**Environmental Magnetism** FCUL-IDL	**MSCL**	**XRF**	**C14** (in progress)	**Pb210**
POPEI	1-1CGG	X	gs (in progress), c, om	χ_{LF}, χ_{FD}, ARM, IRM, NRM, AMS	UBremen	UBremen	Beta	Univ. Bx
	2-1CGP	X	gs, c, om	χ_{LF}, χ_{FD}, ARM, IRM, NRM, AMS	UBremen	UBremen	Beta	Univ. Bx
	15-1CGP	X	gs ((in progress), c, om	χ_{LF}, χ_{FD}, ARM, IRM, NRM, AMS	UBremen	UBremen	Beta	Univ. Bx
MOWER	MW105	x	gs, c, om	χ_{LF}, χ_{FD}, ARM, IRM, NRM	Uvigo	Uvigo	Actalabs	Univ. Bx
	MW106	x	gs, c (in progress), om	χ_{LF}, χ_{FD}, ARM, IRM, NRM	Uvigo	Uvigo	Beta	Univ. Bx
	MW107	x	gs, c, om	χ_{LF}, χ_{FD}, ARM, IRM, NRM	Uvigo	Uvigo	Actalabs	Univ. Bx

3.1. Sedimentological analyses

Grain size analysis was made essentially by laser diffraction particle size analyser Malvern Mastersizer Hydro 2000G, following the necessary protocol and the adequate software, which provides the grain-size data as a volume percentage for all the textural distribution (<0.001µm to 2 mm). Such analyses were performed every cm of core length. In the coarser cores as MW105, MW107 and part of 1-1CGG, a 500µm sediment separation was made in order to make grain-size analysis more representative and reliable. The fraction <500µm was analysed by laser diffraction while the fraction >500µm by classical sieving method.

Carbonate content was analysed in accordance with the volumetric method of Scheibler, as described in Tatzber *et al*. (2007) using an Eijkelkamp calcimeter.

The organic matter content (OM) was determined by loss-on-ignition at 450°C following Craft *et al.* (1991) where 200 mg of each sediment sample during approximately 2 hours in a muffle furnace and the results were expressed as the percentage of total organic matter in each sample.

3.2. Multi-sensor Core Logger data

In all the POPEI and MOWER cores, non-destructive measurements of the petrophysical properties: gamma ray attenuation density (GRA), P-wave velocity (PW) and magnetic susceptibility (MSL) were done. The MOWER cores measurements were done on whole-round cores at the University of Vigo, while the POPEI cores measurements were done in the split section halves at the MARUM – University of Bremen. Measurements were done with a GEOTEK Multisensor Core Logger (MSCL), with a measurements frequency of 1 per cm.

Color reflectance and sections half photograph were measured in all the cores, but in the case of the POPEI cores that had been previously splitted the color measurements could not be done immediately after splitting. Color reflectance properties were converted and are presented in RGB values. The color reflectance spectrometry parameters and the physical property measurements were performed to help characterize the lithostratigraphic units and to describe the cores.

3.3. XRF Core Scanner data

On the MOWER cores, data was collected every 10 mm down-core over a 15 mm^2 area with down-core slit size of 10 mm using generator settings of 30 kV, a current of 55 mA, and a sampling time of 20 seconds directly at the split core surface of the archive half with ITRAX Core Scanner at the University of Vigo. The split core surface was covered with a 4 micron thin SPEXCerti Prep Ultralene1 foil to avoid contamination of the XRF measurement unit and desiccation of the sediment. The here reported data have been acquired and processed by a CoreScanner 8.6.3 with the Q-spec 8.6.0 software package. Identified elements: Al, Si, S, Cl, K, Ca, Ti, V, Cr, Mn, Fe, Ni, Zn, Ga, Ge, As, Br, Rb, Sr, Y, Zr, Cs, Ba, La, Ce, Nd, Sm and Pb (not in all measurements). Due to the low abundance, the elements: Ge, As, Ce, Nd, Sm and Pb should be considered only as indicative.

On the POPEI cores, data was collected every 10 mm down-core over a 15 mm^2 area with down-core slit size of 10 mm using generator settings of 30 kV (1^{st} run) and 10 kV (2^{nd} run), a current of 1.0 mA (1^{st} run) and 0.2 mA (2^{nd} run), and a sampling time of 20 seconds directly at the split core surface of the archive half with XRF Core Scanner II (AVAATECH Serial No. 2) at the MARUM - University of Bremen. The split core surface was covered with a 4 micron thin SPEXCerti Prep Ultralene1 foil to avoid contamination of the XRF measurement unit and desiccation of the sediment. The here reported data have been acquired by a Canberra X-PIPS Silicon Drift Detector (SDD; Model SXD 15C-150-500) with 150eV X-ray resolution, the Canberra Digital Spectrum Analyzer DAS 1000, and an Oxford Instruments 50W XTF5011 X-Ray tube with rhodium (Rh) target material. Raw data spectra were processed by the analysis of X-ray spectra by Iterative Least square software (WIN AXIL) package from Canberra Eurisys. Identified elements with realiable confidence for scientific publications: Al, Si, S, K, Ca, Ti, Mn, Fe, Br, Rb, Sr, Zr, Pb. Due to the low abundance, the elements: Ni, Cu, Zn, Ga, Nb, Mo, Bi, P, Cl, Rh and Cr should be considered only as indicative.

Due to the high reliability of the Ca and Ti elemental quantification, elements are in in general normalized for Ca and for Ti.

3.4. Magnetic analyses

3.4.1. Magnetic analyses of offshore sedimentary cores

Environmental magnetism experiments were conducted each centimeter of the cores through the use of cylindrical samples with one centimeter of diameter and two of height (volume ~ 1.6 cm^3). Experiments comprise measurements of: i) Thermomagnetic experiments - *K(T)* conducted between -190ºC and 650ºC (cryostat CS-L and furnace CS-4 coupled with MFK1-FA; high temperatures experiments conducted under Argon controlled atmosphere); ii) low-field mass normalized magnetic susceptibility (χ_{lf}) (MFK1 kappabridge); iii) anhysteretic remanence (ARM), acquired through a direct field of 50 µT under the application of an alternating demagnetization field with peak of 100 mT (JR6 to measure the remanence and LDA coupled with AMU-1 for the ARM acquisition); iv) acquisition of IRM at 1 and 2 T and latter acquisition of backfields at 0.1 T and 0.3 T; and v) gradual acquisition of IRM until a maximum applied field of 5 T. All results were mass normalized.

Anisotropy of magnetic susceptibility and natural remanent magnetization (NRM) vector were evaluated for cubic samples (8 cm^3) collected every three to five centimeters. For the determination of NRM vector was used the JR6 (AGICO) magnetometer. Some samples were also submitted to alternating magnetic demagnetization (LDA demagnetizer, AGICO) up to fields of 100 mT in order to check the NRM stability. After all these measurements all cores were rotated to a common northward frame. The AMS ellipsoid was determined through measurements in the MFK1 kappabridge (AGICO). Degree of anisotropy, shape and preferential orientation of the magnetic susceptibility ellipsoid were then determined.

2.4.2. Magnetic analyses of onshore sediments

In order to inspect the typical magnetic mineralogy present in the Algarve coast, able to be eroded and transported towards offshore domains, two samples of poorly consolidated Pliocene-Quaternary reddish sands that commonly cover the Miocene cliffs of Algarve coast were here analyzed by thermomagnetic and IRM means.

4. RESULTS

4.1. Description

Sediments of POPEI and MOWER cores are mostly fine grained, very homogenous, structurless, with no visible lamination and are very bioturbed (Figures 2 and 3). Sediment colour vary usually between light olive gray (5y 5/2) to olive gray (5Y3/2). Sediment becomes coarser towards base with many fragments shells.

The POPEI and MOWER cores show a typical transgressive succession with increasing energy depositional regimes from the top to the bottom of the cores (Figures 2 and 3).

The base of the MOWER cores (from 210 to 250 cm in MW105, from 320 to 360 cm in MW106 and from 20 to 120 cm in MW107) is a very coarse sand with chaotic massive and unstructured facies, very rich in large shells and shell fragments (Figure 3).

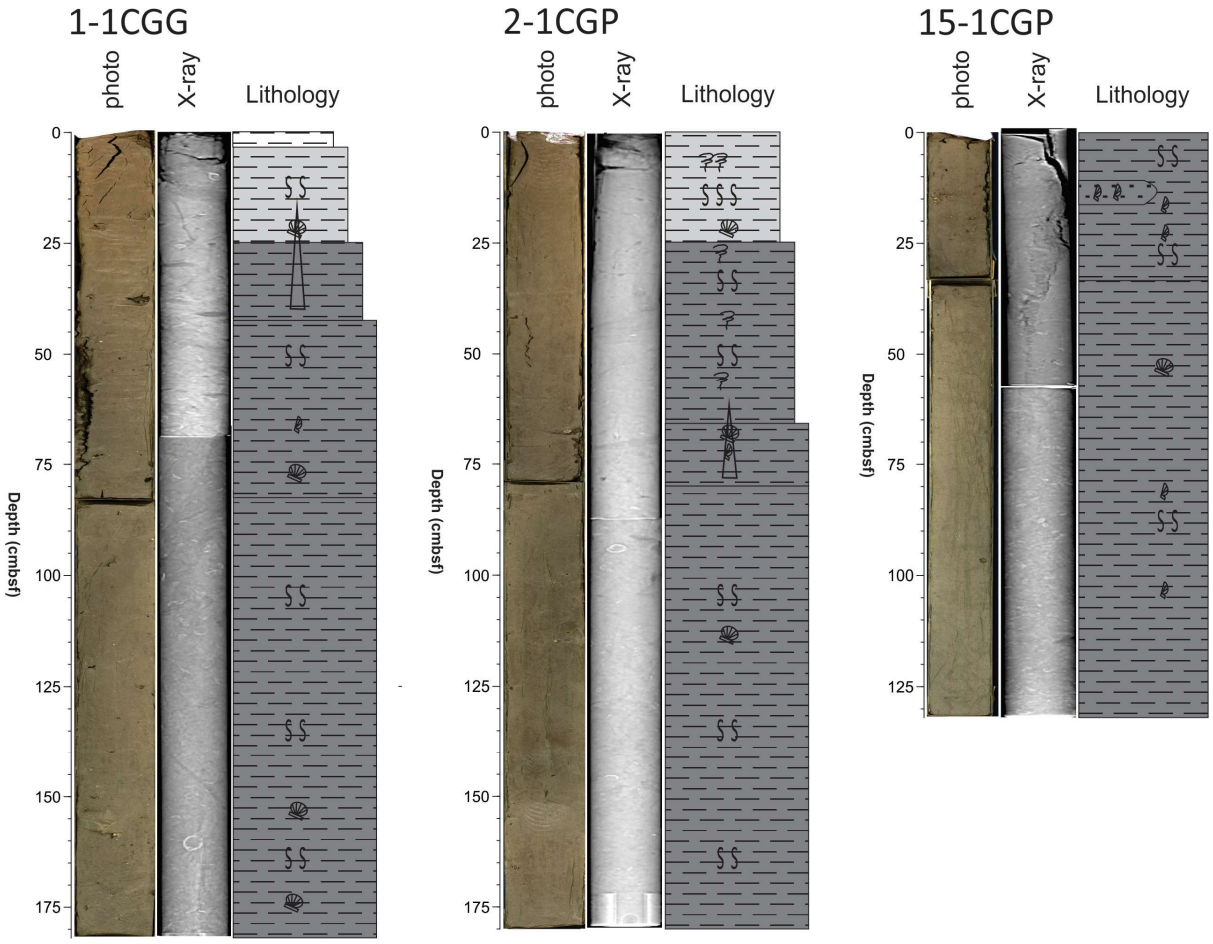

Figure 2 - X-ray, photo and visual description log of the POPEI cores.

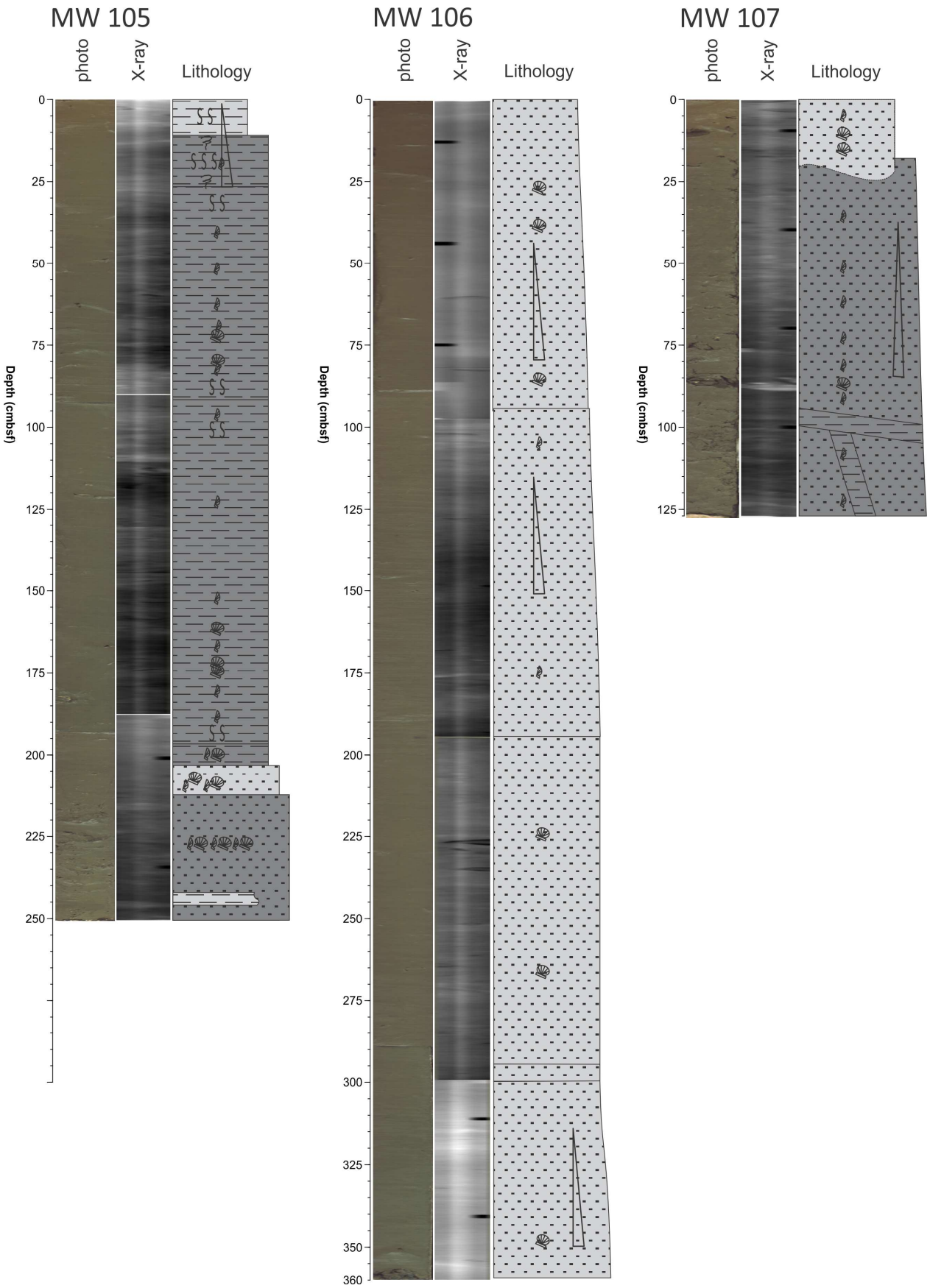

Figure 3 - X-ray, photo and visual description of the three MOWER cores.

4.2. Sedimentology

- Mean grain size profiles show decreasing trends towards the top, which is always finer than the base. This is particularly well expressed in all the analyzed cores (exception for 15-1CGP, which grain-size analysis is still in progress) (Figures 4a-9a). In 1-1CGG, 2-1CGP and MW106 cores, the mean grain size show values from 50µm at base to 20-10µm at top (Figures 4a, 5a and 8a), while in MW105 and MW107, the base is clearly coarser, showing mean grain sizes of 200-600µm (Figures 7a and 9a).
- Textural types contents of the cores 1-1CGG, 2-1CGP and MW106 show the clearly predominance of silt, with percentages of 40-70% (Figures 4b, b and 8b). However, in MW105 and MW107, sand becomes predominant (50- 75%) deeper than 220cm and 40cm respectively (Figures 7b and 9b). Clay present variations between 25% and 10% in 1-1CGG and 2-1CGP (Figures 4b and 5b) and between 30-20% in MW106 (Figure 8b). Gravel is also present in cores MW105 and MW107, with percentages that can attain 10% (Figures 7b and 9b).
- Carbonates contents follows the grain-size trend, as an expression of the shells and shell fragments content in the sand textural type. For 1-1CGG and 2-1CGP, the carbonates contents are very similar and varying between 8-14% (Figures 4c and 5c). MW105 and MW107 cores, constituted by coarser sediments especially at the base, present also higher carbonates (15-25 and 15-30%, respectively) (Figures 7c and 9c). Regarding 15-1CGP core, sampled offshore Sagres, seems to be coarser than the others, as deduced from the carbonates contents, varying from 35 to 45% (grain size in progress, not finished) (Figure 6c).
- Organic matter is related to fine sediments, showing an inverse behavior of mean-grain size/carbonates (Figures 4d-9d). Normally, this parameter does not exceed 10%. However, in core 1-1CGG, it can attain values of 12% and in core 15-1CGP, doesn't exceed 6% (Figures 4d and 6d).

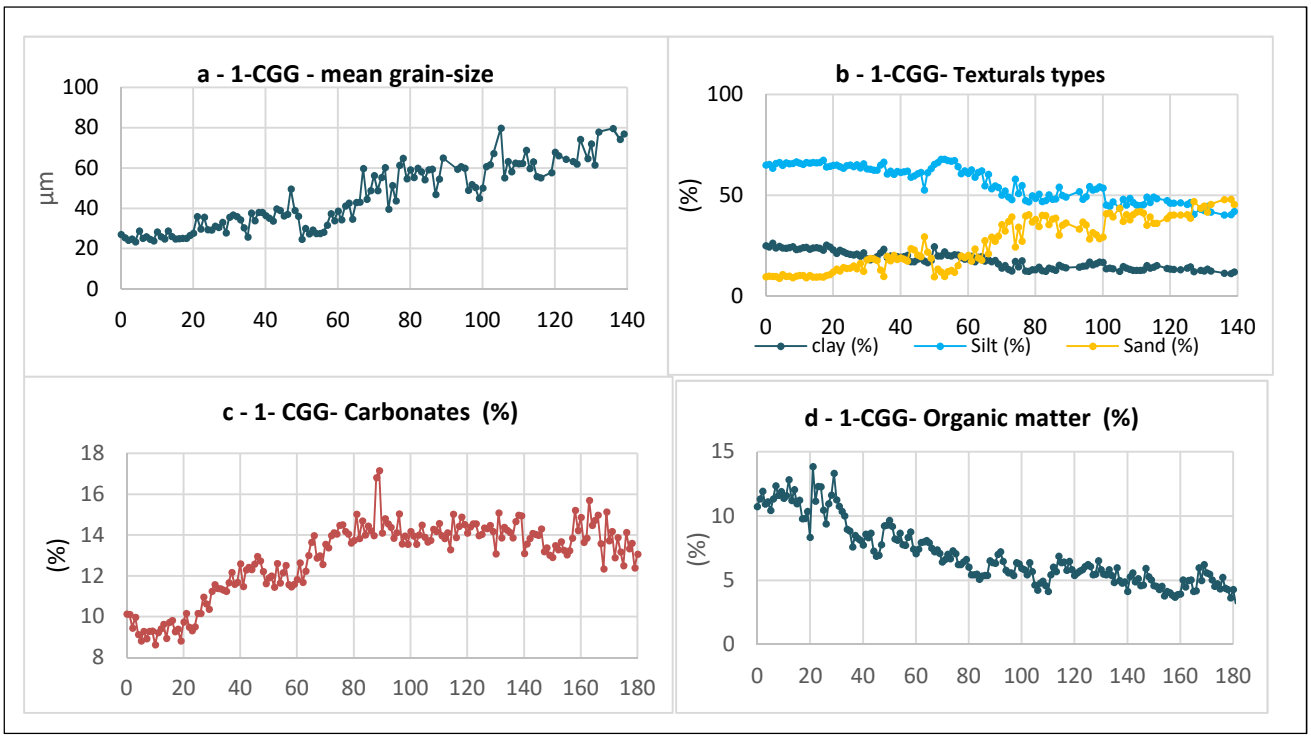

Figure 4 - POPEI 1-1CGG -Grain size analysis: mean grain size (µm) (a), texturals types (sand, silt and clay (%) (b), carbonates (c) and organic matter contents (d) (%).

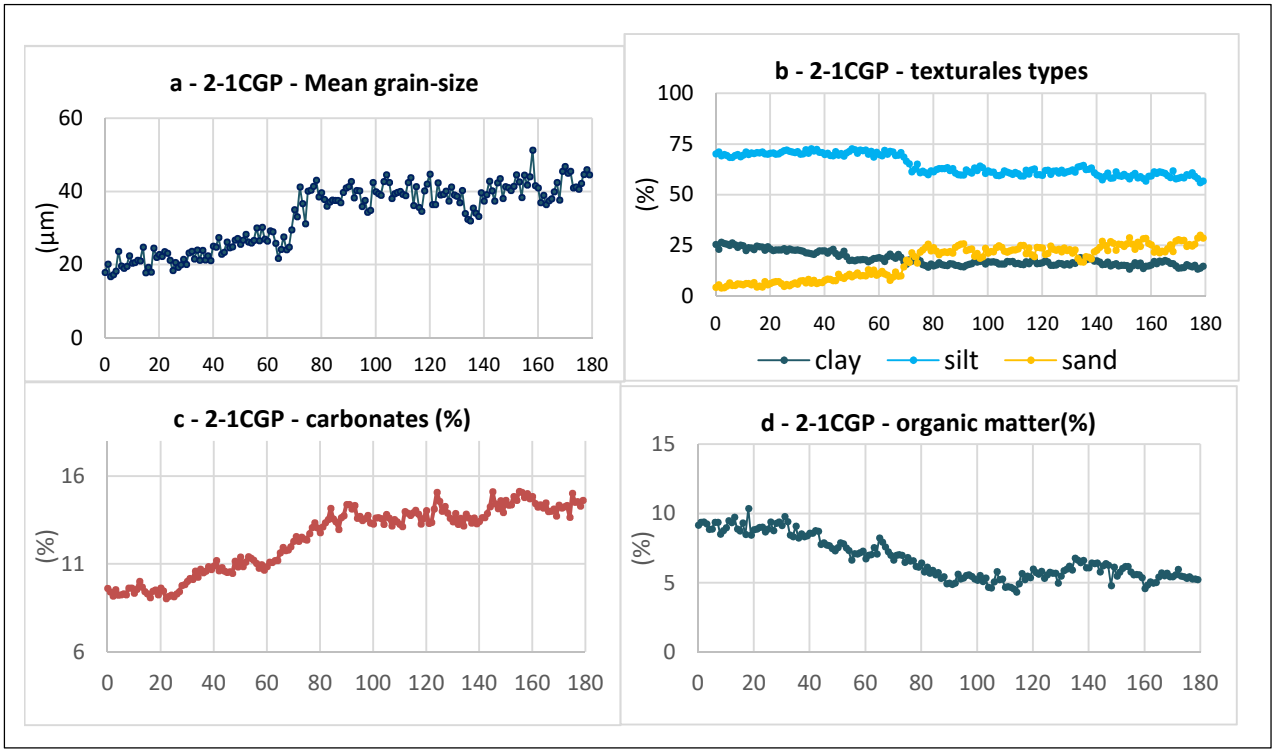

Figure 5- POPEI 2-1CGP- Grain size analysis: mean grain size (µm) (a), texturals types (sand, silt and clay (%) (b), carbonates (c) and organic matter contents (d) (%).

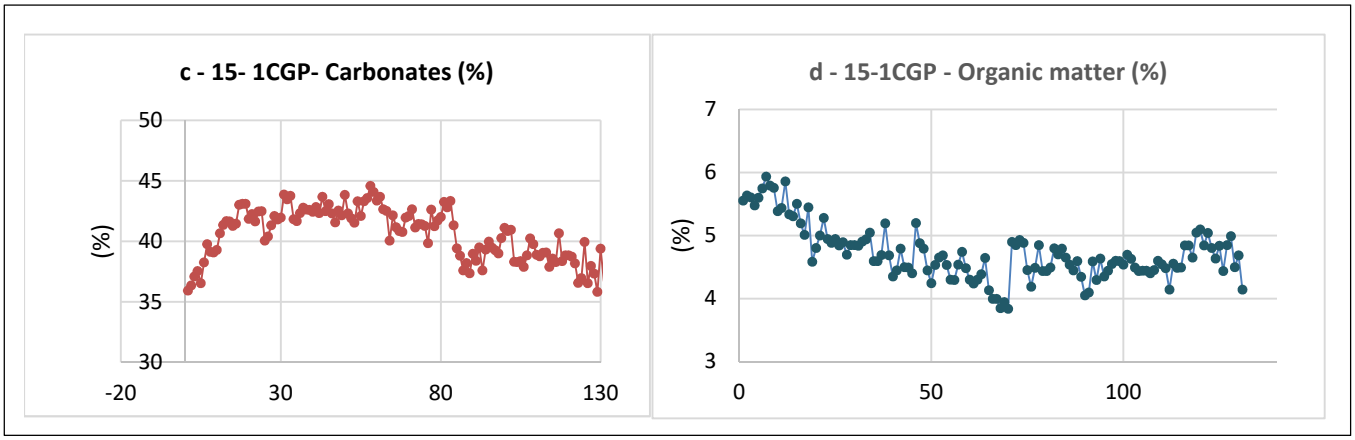

Figure 6 - POPEI 15-1CGP- carbonates (c) and organic matter contents (d) (%). Grain-size analysis is in progress.

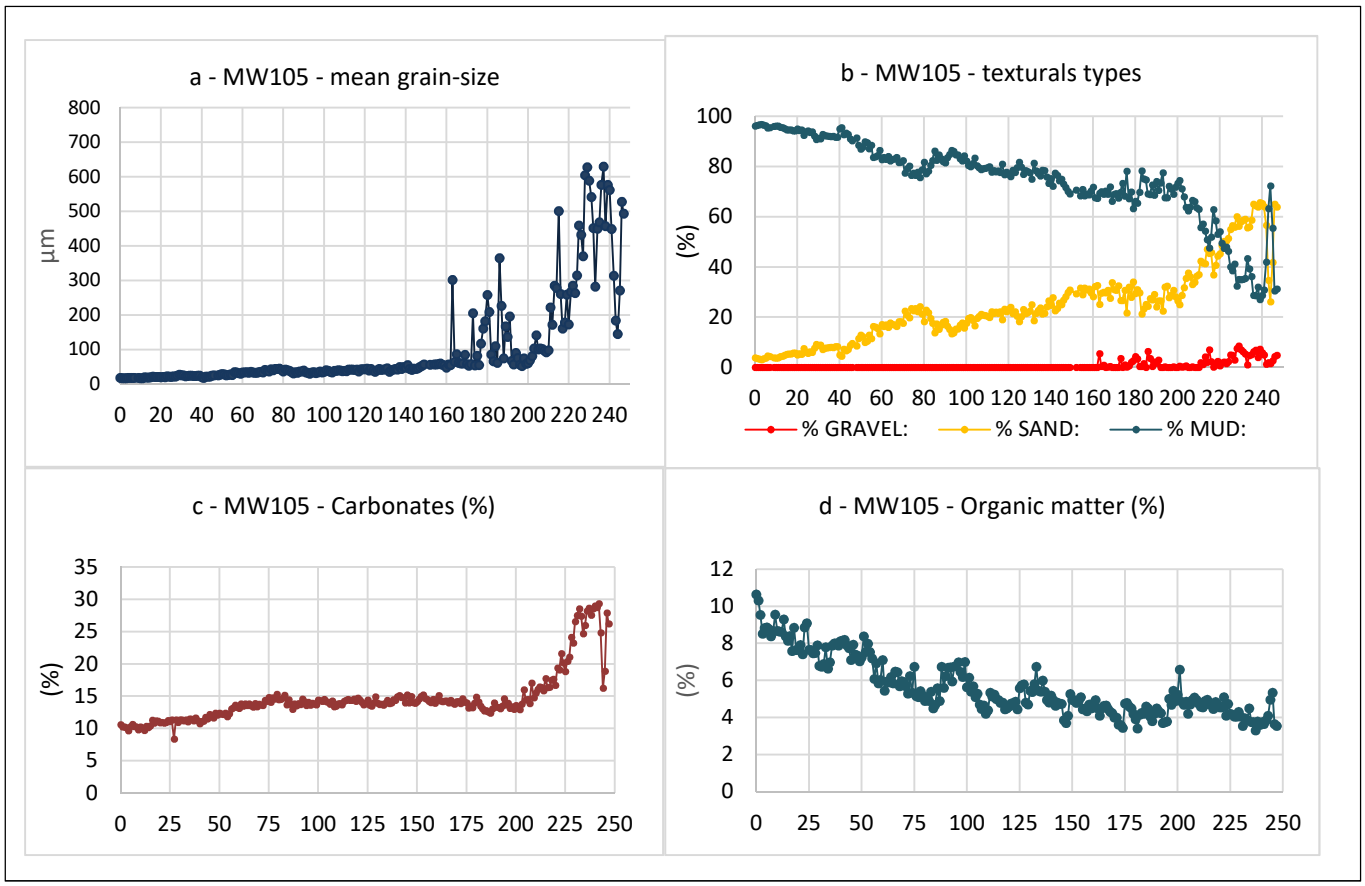

Figure 7 - MOWER105 - Grain size analysis: mean grain size (µm) (a), texturals types (gravel, sand and mud (silt+clay)) (%) (b), carbonates (c) and organic matter contents (d) (%).

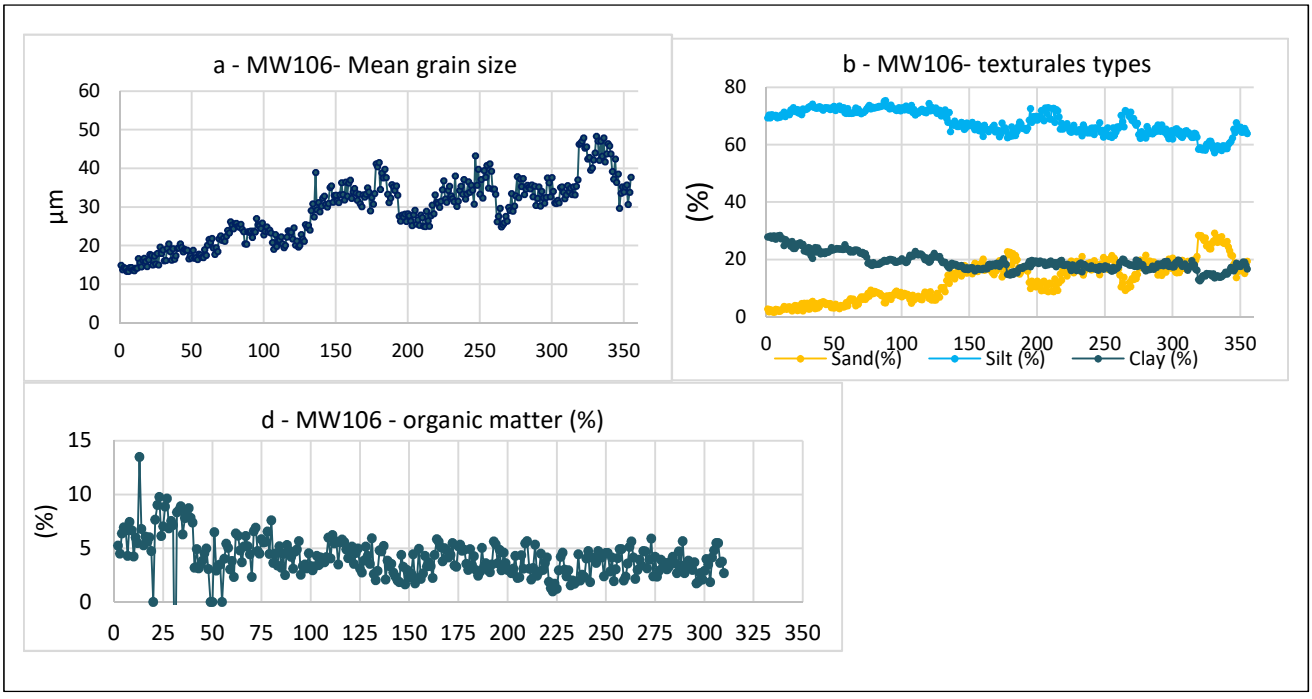

Figure 8 - MOWER106 - Grain size analysis: mean grain size (µm) (a), texturals types (sand, silt and clay (%) (b), carbonates (c) and organic matter contents (d) (%).

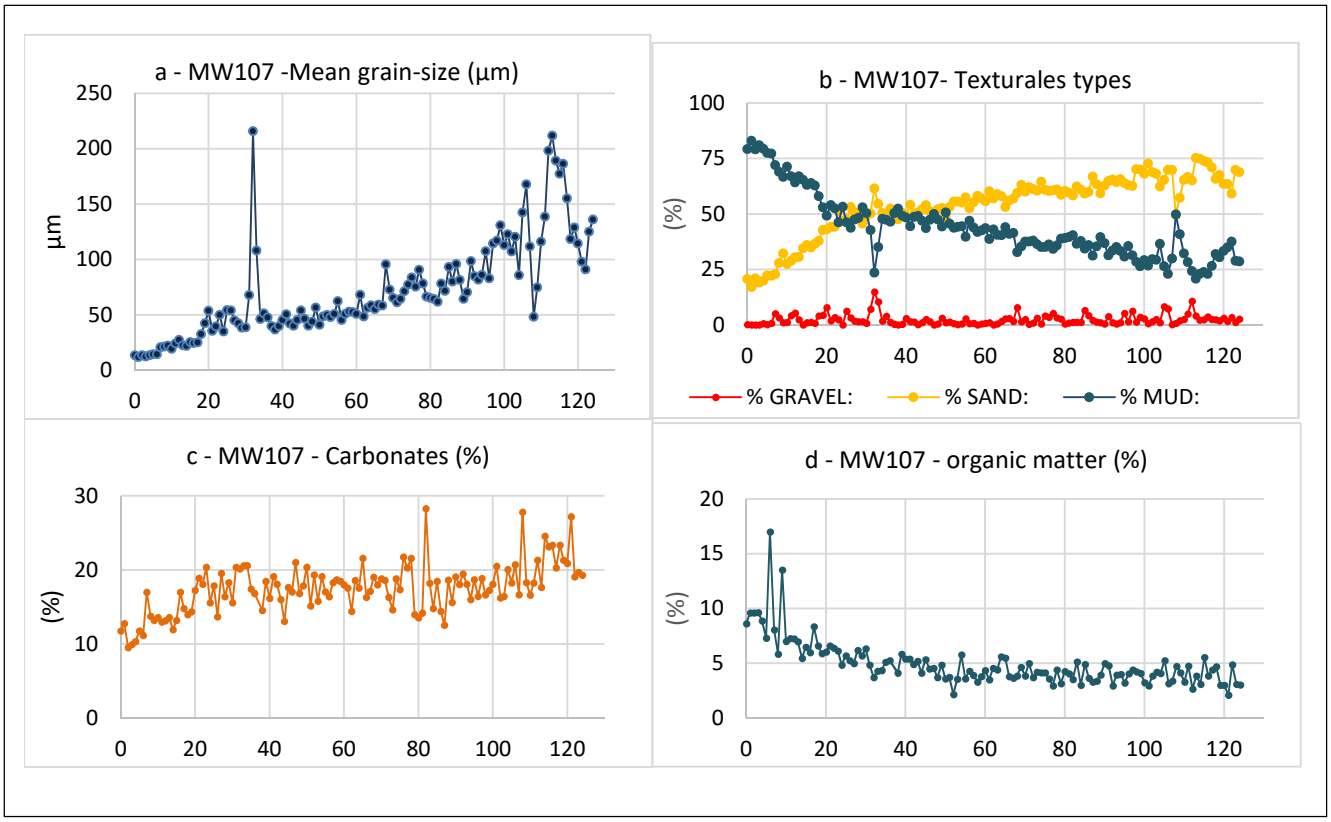

Figure 9 MOWER 107 - Grain size analysis: mean grain size (µm) (a), texturals types (gravel, sand and mud (silt+clay)) (%) (b), carbonates (c) and organic matter contents (d) (%).

The mean grain-size comparison of the studied cores, show that this parameter are for the mostly of them below 50 µm(Figure 10). However, as it can be observed, MW105 and MW107 cores are coarser than the others, especially at base where mean grain sizes have values of 200-600 µm.

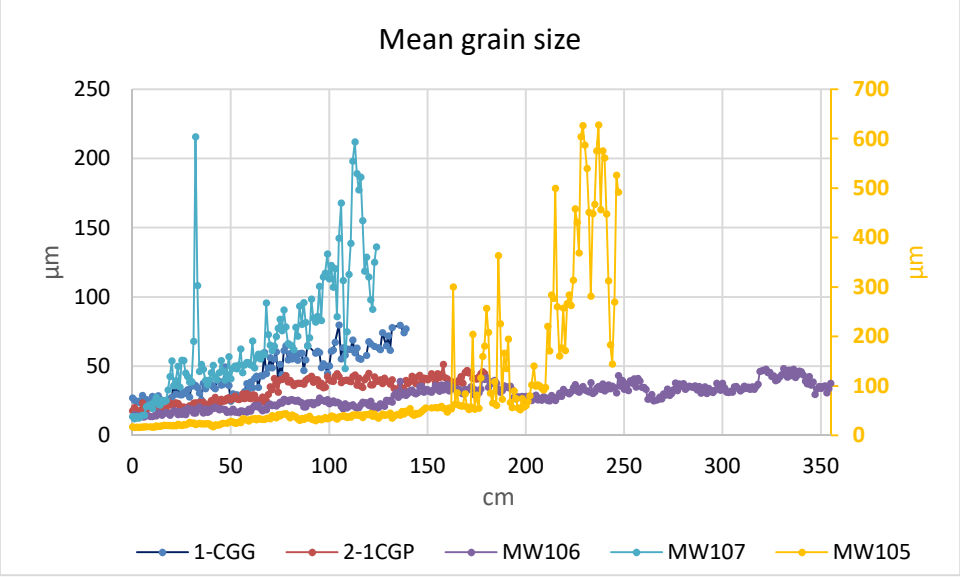

Figure 10 – Mean grain sizes comparison of the POPEI and MOWER cores.

4.3. Magnetism

4.3.1. Main magnetic phases of onshore Pliocene-Quaternary reddish sands

For the samples collected at southern Portuguese coast (Figure 11a), thermomagnetic analyses – K(T) at low temperatures show a gradual decrease of K up to -50ºC (Figure 11b), followed by an increase in two steps up to room temperature. Such increase likely resembles the Morin transition – T_M of the antiferrimagnetic hematite, despite for temperatures lower than the expected -15ºC.

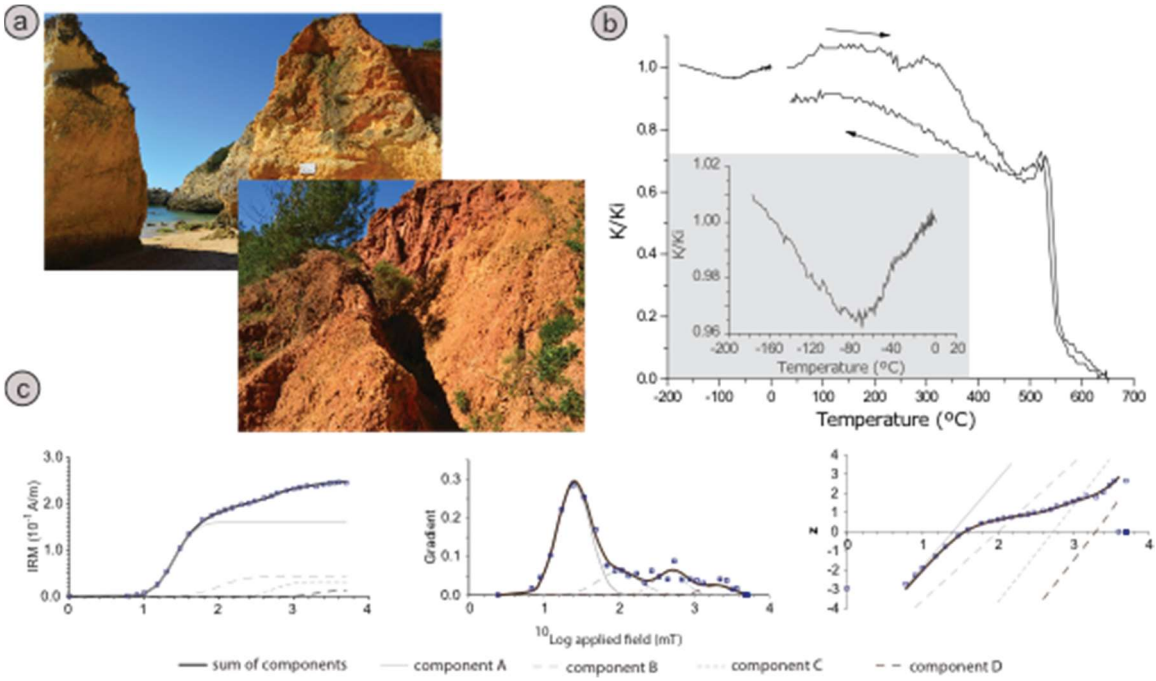

Figure 11 - a) Pictures from the southern coast of Portugal, showing the typical reddish colored sediments; b) Thermomagnetic measurements conducted under argon controlled atmosphere; c) Cumulative log-Gaussian analyses (Kruiver *et al*. 2001) conducted for representative samples.

According to Ozdemir *et al*. (2008) and Mitra *et al.* (2009) this shift could be explained by the dependence of T_M in function of the dominant grain size and shape of hematite. At higher temperatures is visible a small increase of K around 200ºC followed by a decrease between 230 and 270ºC. Such decrease agrees with the thermomagnetic characteristics of hexagonal pyrrhotite (Schwarz, 1975; Evans and Heller, 2003). Above, it is observed a gradual decrease of K values that invert to an increase around 500ºC, defining a peak at 530ºC. Such peak is interpreted as an Hopkinson effect due to superparamagnetic behavior of tiny (Ti)magnetite grains. From 530 to 650ºC K values decrease in two-steps, abruptly from 530 to 560ºC and more gently above. Such two drops suggest the presence of Ti-magnetite poor in titanium (Curie temperature of 550ºC) and hematite. Despite the thermomagnetic cycle is irreversible, the difference between heating and cooling curves at 40ºC is only 10%, indicating the occurrence of moderate mineralogical changes during the experimental procedure (Hrouda *et al*., 2006).

IRM measurements of both samples show similar IRM acquisition, being able to identify four components with distinct coercivities (Figure 11c). Approximately 55% of IRM signal is due to the magnetic phase with lower coercivity (saturating for fields around 150 mT). This signature agrees with the presence of (Ti)magnetite and/or its oxidized member. The remaining IRM is carried by magnetic phases with higher coercivity. 20% of the IRM intensity is carried by magnetic phase that saturates at 400 – 600 mT, which agrees with the presence of pyrrhotite (Clark, 1984; Dekkers, 1988). The remaining 25% of the signal is carried by a

magnetic phase that saturates at 1.5-1.7 T (20%) and around 4.0 T (5%), which is consistent with the presence of hematite (Lowrie and Heller, 1982, O'Reilly, 1984).
Therefore, both rock magnetic methods are consonant in the identification of the main magnetic phases. Knowing that the spontaneous magnetization of magnetite (or maghemite) is five times higher than the one of pyrrhotite and approximately 200 times than the one of hematite (e.g., Evans and Heller, 2003), we can conclude that such samples are fairly rich in magnetic phases with high coercivity.

4.3.2. Down-core main magnetic phases

Gradual acquisition of IRM was conducted for the two cores, which according to geochronological data encompass the greater temporal interval, namely, MW14-GC-105 (14 samples analyzed) and MW14-GC-107 (12 samples analyzed).
IRM cures of both cores are quite similar (cf. Fig. 12a and b), mainly characterized by a pronounced increase of IRM up to fields of 100 mT, after what shows slighter but gradual increase up to the maximum applied filed of 5 T.
The cumulative log-Gaussian analyses (Robertson and France, 1994; Kruiver *et al*., 2001) of such IRM curves indicate the presence of four main magnetic phases with distinct magnetic coercivities (Figure 12c):

- Component A, represents the component with the lowest coercivity, showing half-saturation fields ($B_{1/2}$) around 20 mT. The achieved coercivity values agree well with the values expected for the iron-oxides, magnetite and/or its oxidized member, maghemite (e.g., Dunlop and Ozdemir, 1997). This component is responsible for approximately 30% of the IRM signature;
- Component B, presents $B_{1/2}$ around 50 mT and their IRM saturates (SIRM) around 300 mT. This signature could be also attributed to the presence of iron-oxides, magnetite and/or maghemite. This component is approximately responsible for 50% of the IRM signal.
- Component C, presents $B_{1/2}$ around 500 mT and their IRM saturates (SIRM) around 1500 mT. This signature could be attributed to the presence of iron-sulfides, pyrrhotite (Clarck, 1984; Dekkers, 1988) and/or greigite (Liu et al., 2012) and/or the iro-oxide, hematite (Dunlop and Ozdemir; 1997). This component is approximately responsible for 10-15% of the IRM signal.
- Component D, corresponds to the one with the highest coercivity, with $B_{1/2}$ values around 2000 mT, but without clearly reaching the saturation up to fields of 5000 mT. Such values point to the presence of high coercivity magnetic phases, must likely, the iron-oxide hematite and/or the oxyhydroxide goethite (Dunlop and Ozdemir; 1997; Rochette *et al*., 2005).

In summary, IRM studies, point to the presence of magnetite and/or its oxidized member, maghemite, as the main magnetic phases, with approximately 80% of the IRM signal. For the remaining signal, there are several hypothesis, namely, hematite, pyrrhotite, greigite and/or goethite.

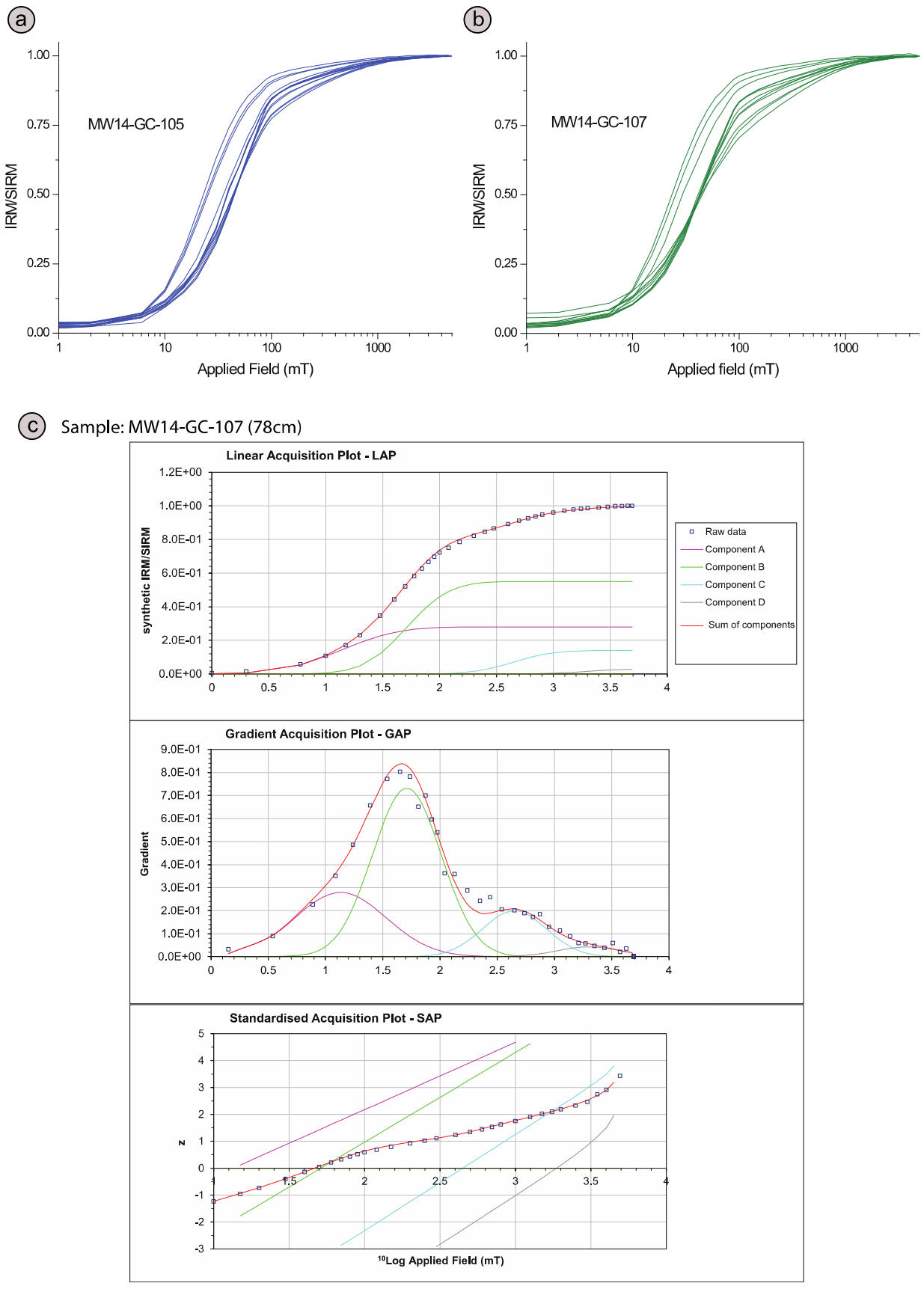

Figure 12 - a) and b) acquisition of IRM; c) Cumulative log-Gaussian analyses (Kruiver *et al*. 2001) for a sample collected at 78 cm from core MW14-GC-107. LAP, Linear Acquisition Field; GAP, Gradient acquisition Plot; SAP, Standardized Applied Field.

4.3.3. Down-core profiles of environmental magnetic parameters

The linear correlation between χ_{LF} and IRM (Figure 13) and the down-core similar patterns between χ_{LF}, IRM and ARM (Figures 14 a,b) indicate that χ_{LF} variations are mostly sensitive to the concentration of ferromagnetic minerals (*s.l.*; hereinafter called magnetic minerals for simplicity).

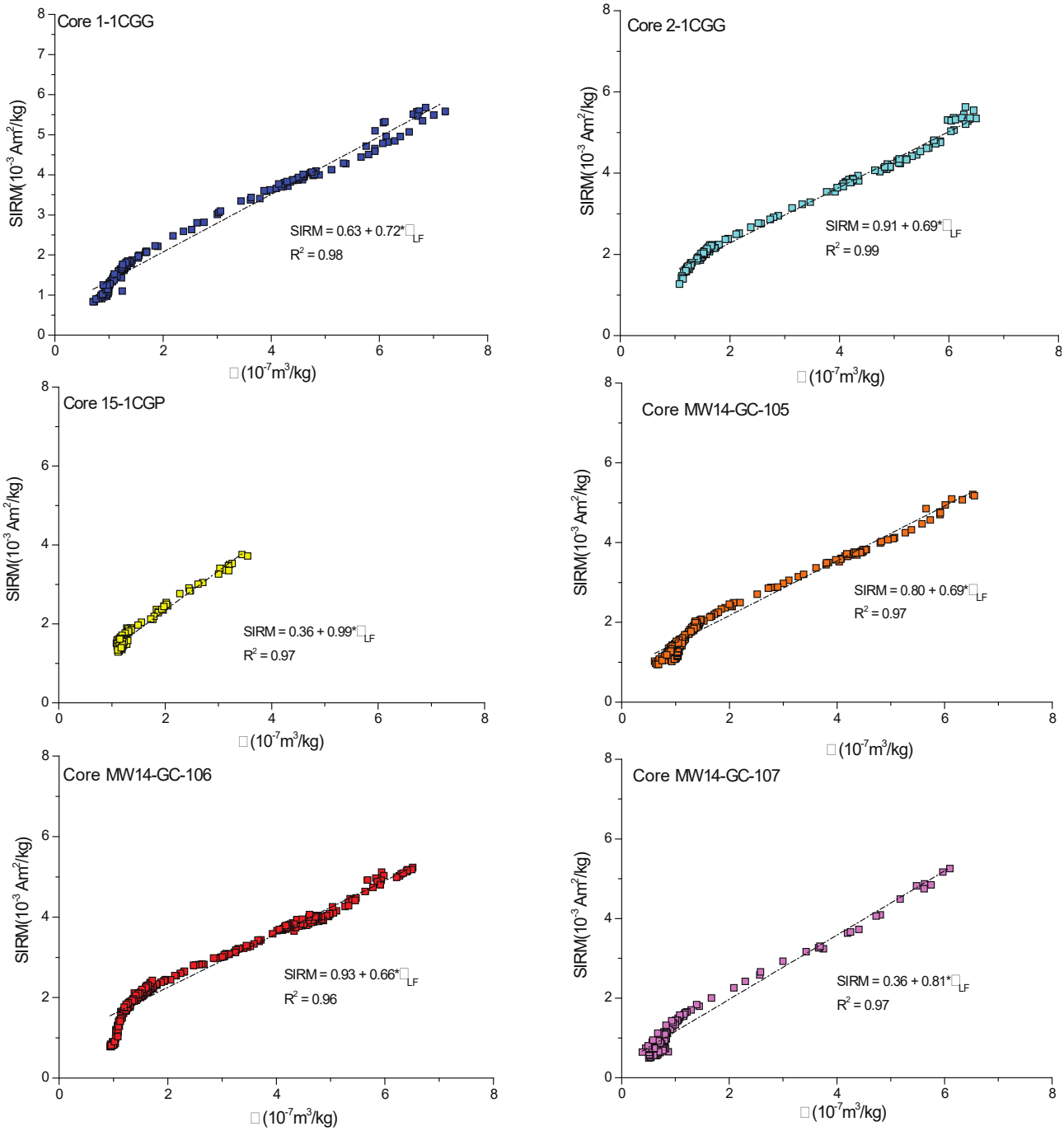

Figure 13 - Comparison between □LF and IRM and respective linear fits

The down-core evolution of magnetic parameters sensitive to the concentration of magnetic minerals (χlf, ARM IRM), their magnetic granulometric state (ARM/IRM and □ARM/□LF), relative contribution between soft and hard components (S-ratio), and superparamagnetic behavior (χFD) enables the identification of four main long-term magnetic units, with limits that vary between cores (Figures 14). From top to down, such magnetic

units are M1, M2, M3 (not observed for cores POPEI-2 and POPEI-15) and M4 (this one only observed for cores MW14-GC-105 and MW14-GC-107).

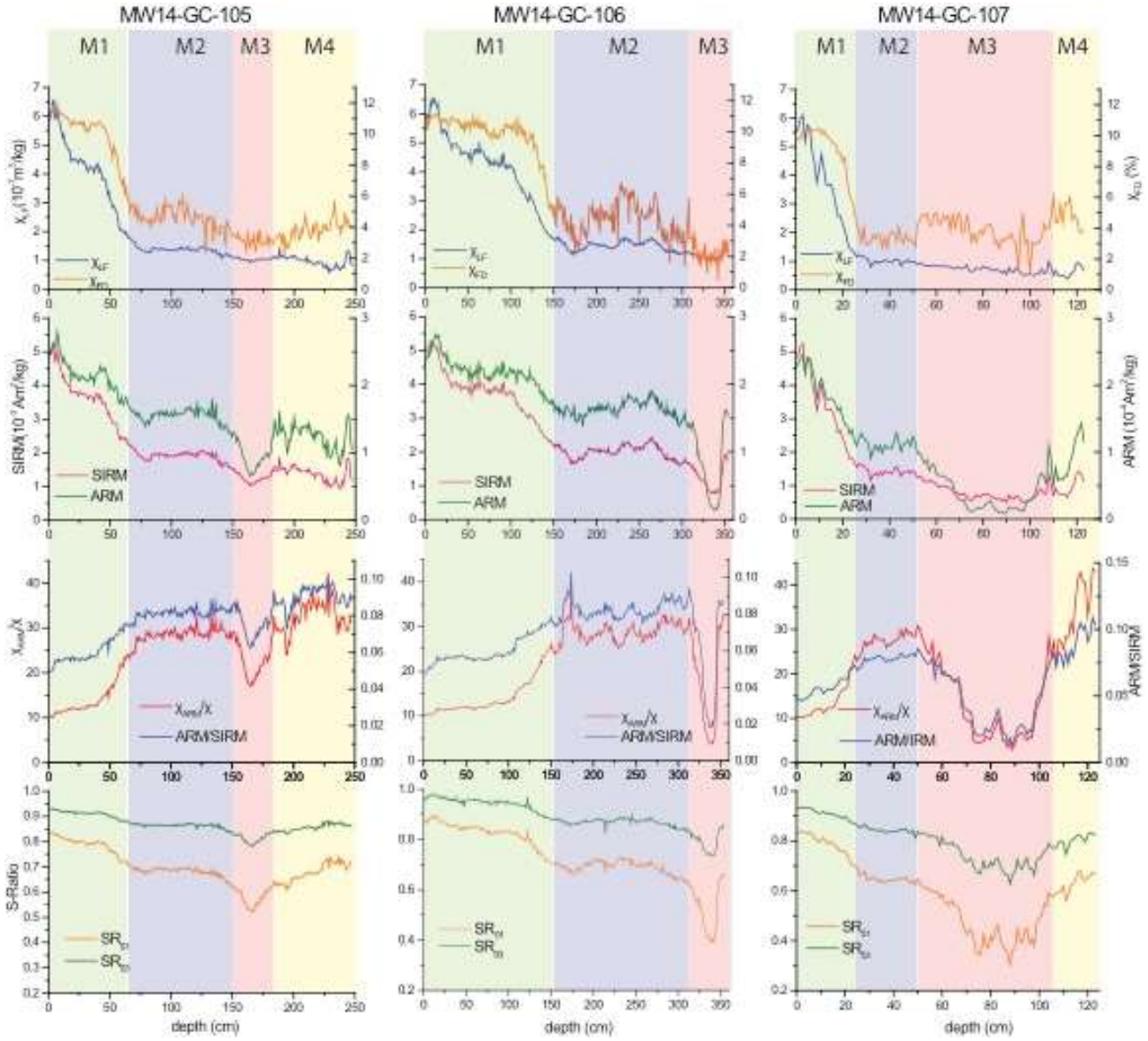

Figure 14 – Evaluation of several environmental magnetism parameters and their ratios along cores depth. χ_{lf} – mass normalized low field magnetic susceptibility; IRM - isothermal remanent magnetization; χ_{ARM} – susceptibility of anhysteretic remanent magnetization; S-Ratios acquired by back fields of 100 mT ($SR_{0.1}$) and 300 mT ($SR_{0.3}$) after application of a direct field with 2T; χ_{FD} (%) percentage of magnetic susceptibility frequency dependence.

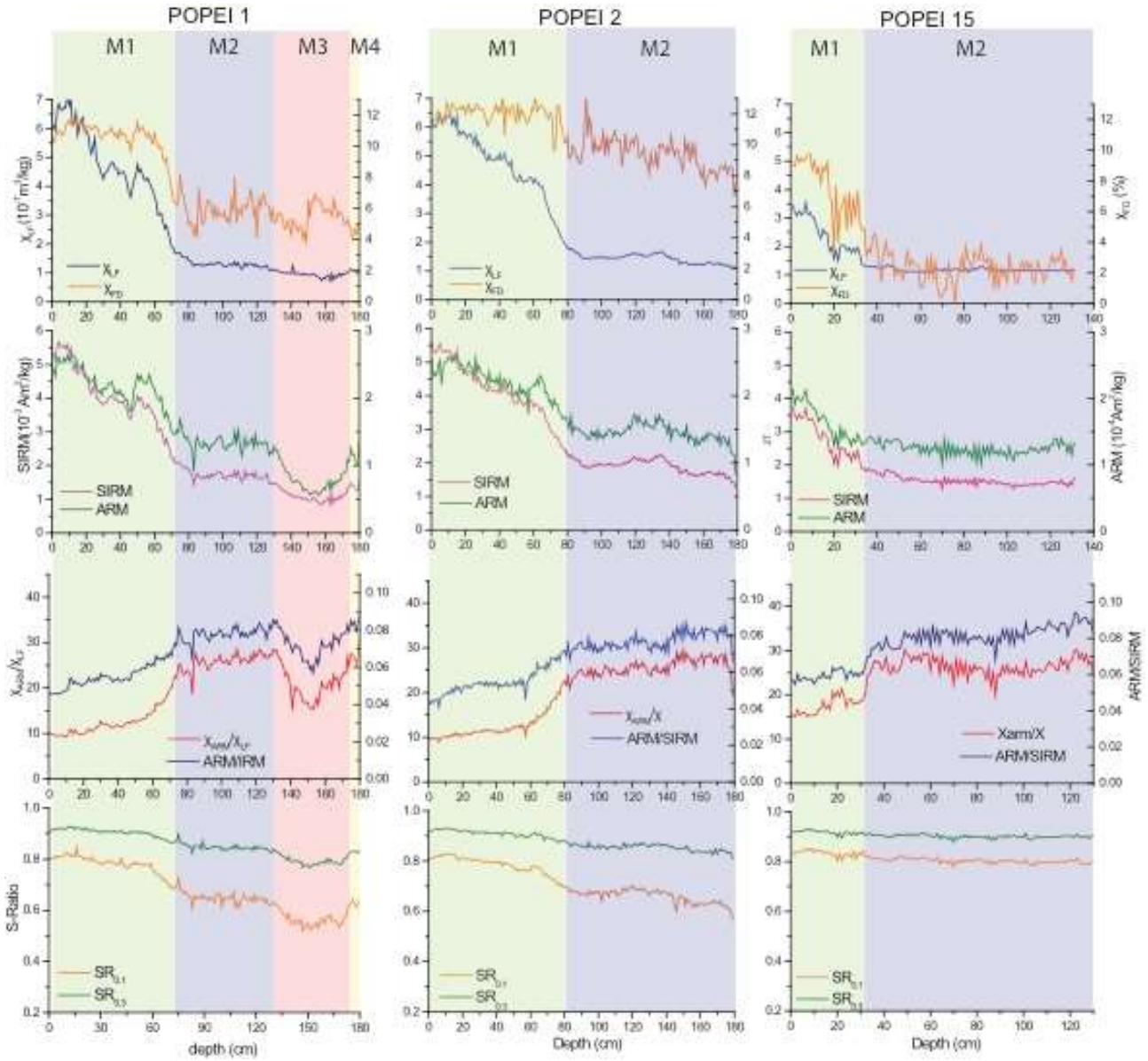

Figure 14 – continuation.

- **Unit M1**, which corresponds to the upper one, is characterized by a well-marked decrease of the magnetic minerals concentration towards its base, as shown by profiles of parameters χ_{lf}, ARM and IRM. A "plateau" of stable values or even a decrease commonly interrupts this decrease. This trend is closely followed χ_{FD} and S-ratio. Otherwise, parameters sensitive to the magnetic granulometry state show an inverse evolution, which agrees with an overall increase of the magnetic granulometric state of the main magnetic carrier, except when magnetic parameters sensitive to the concentration stabilize at the "plateau". Here, the magnetic granulometric state shows a slight decrease;

- **Unit M2**, is mostly characterized by low amplitude oscillations in turn of a stable average value of all the magnetic parameters here analyzed, pointing for stable concentration and magnetic granulometry of the main ferromagnetic carriers;

- **Unit M3**, is mostly characterized by stable χ_{FD} values in turn of a mean value of 3 to 5%, depending of the cores. Such stability indicates a quite homogeneous granulometry of the main magnetic carriers. χ_{lf} show low values with some minor oscilations. The remaining parameters are able to identify a remarkable negative peak, defining a V-shape, which goes mostly unnoticed by χ_{lf} and χ_{FD}. This feature cannot be directly correlated with magnetic granulometry once for this sedimentary interval is observed an increase of the hard magnetic fraction relative to the soft one (cf. S-ratio evolution). All together these parameters indicate a decrease of the concentration of the low coercivity magnetic phase (as seen from the decrease of IRM values) with a relative

increase of the hard fraction (as visible from the low capacity of the hard fraction in acquire anhysteretic remanence under the application of low intensity magnetic fields).

- **Unit M4**, is only observed for half of the cores. It is characterized by significant oscillations of parameters sensitive to the magnetic granulometry state, while parameters sensitive to concentration of ferromagnetic carriers are quite stable, with exception of ARM. ARM despite considered a parameter sensitive to concentration, it is strongly dependent of the magnetic coercivity, and so, justifying its good agreement with magnetic variation observed for parameters sensitive to the magnetic coercivity.

4.3.4. NRM Directions

The segments of each core were rotated to the same frame according to the mean direction of natural remanent magnetization. After rotation, cores POPEI-1 and POPEI-2 mostly show a Fisher distribution around the mean direction (Figure 15). However, each core shows a segment where inclination values decrease significantly. For core POPEI-1such segment is achieved between 75 and 101 cm and for core POPEI-2 is observed between 33 and 54 cm. In what concerns core POPEI-15, it is observed a sharp variation of declination and inclination from 66 to 69 cm depth. Sharp variations are also observed from 135 to 138 cm at core MW14-GC-106 and from 87 to 90 cm at core MW14-GC-105.

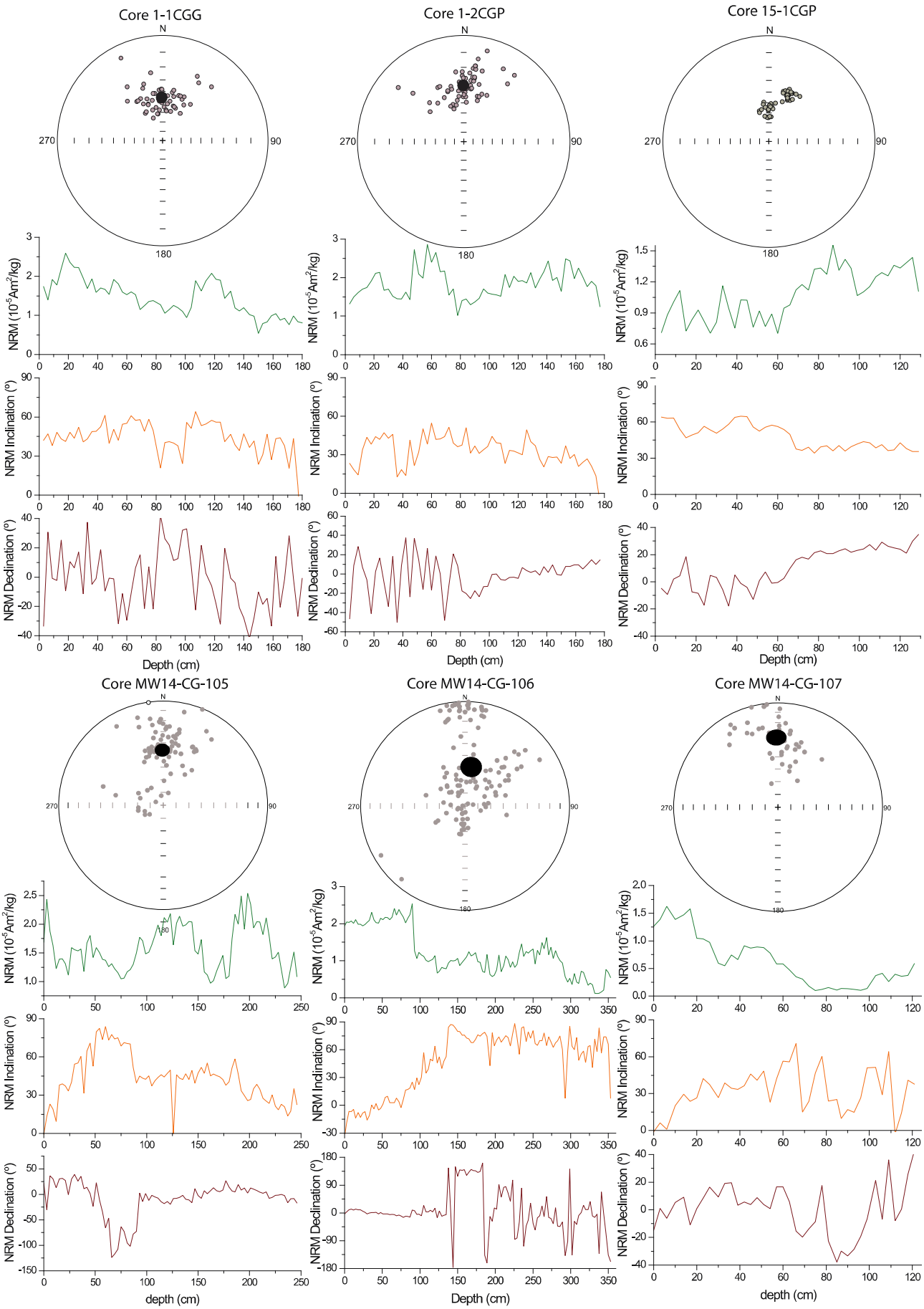

Figure 15 - Data obtained from measurements of natural remnant magnetization - NRM.

4.3.5. Magnetic Fabric

Magnetic fabric measured for three of the six cores mostly show a typical sedimentary fabric, i.e., minor axis (pole of the magnetic foliation) sub-vertical, defining a sub-horizontal magnetic foliation (Figure 16). The degree of anisotropy of the magnetic susceptibility ellipsoid is low (Pj < 1.05) and its shape is mostly oblate. However, there are some sedimentary intervals where the shape departs consistently (i.e., more than one data point) from oblate to prolate. Such transitions are observed for core POPEI 2 between 20 and 30 cm, and between 50 and 80 cm. At these intervals are also verified a decrease of K3 inclinations. K1 is mostly sub-horizontal for all cores, N-S aligned for core POPEI-1, NW-SE for core POPEI-2 and without a conclusive preferential alignment for core POPEI-15.

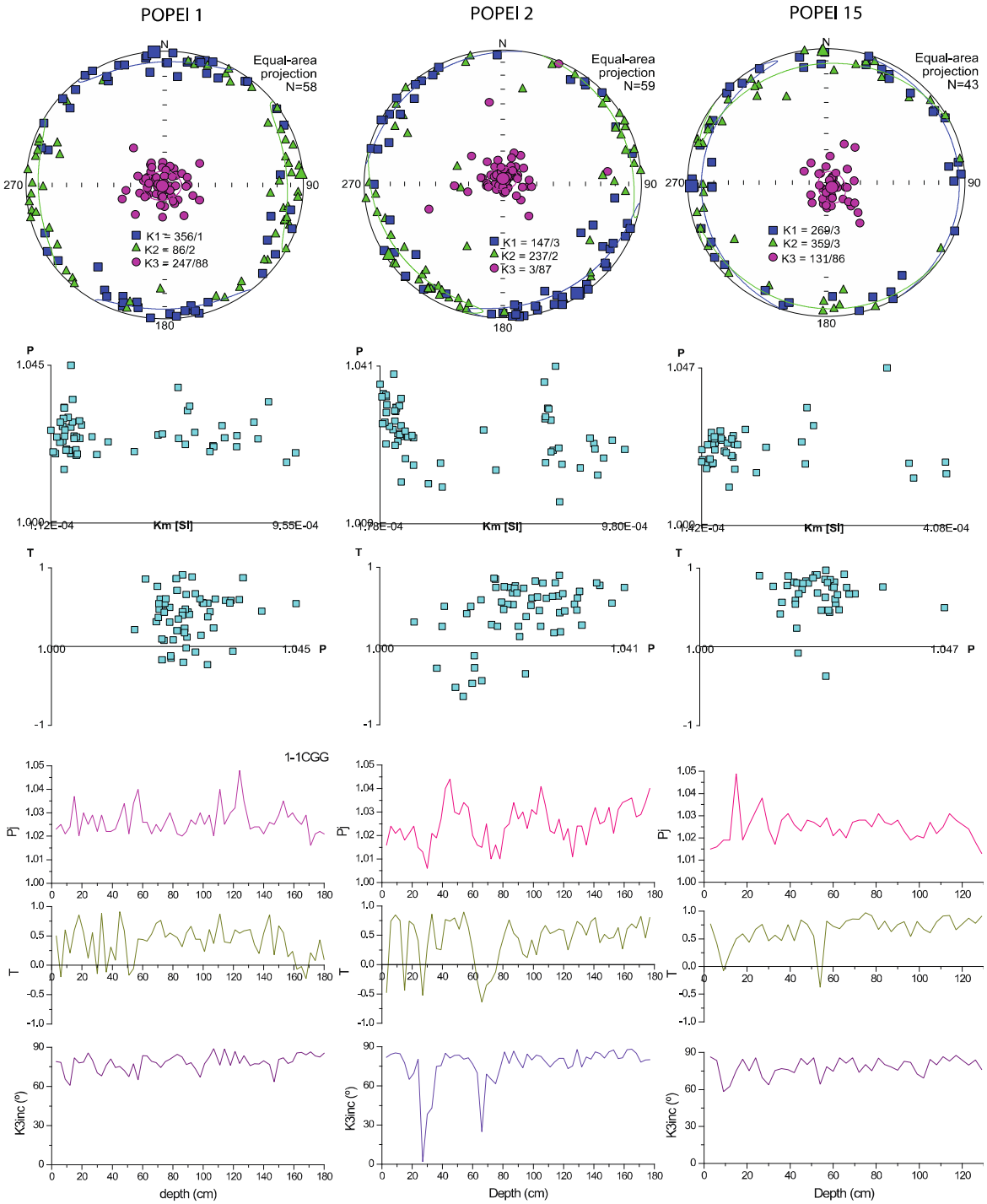

Figure 16 - Data obtained from measurements of anisotropy of magnetic susceptibility – AMS.

4.4. – Multi-Sensor Core Logger data

In the following figure it is represented the MSCL measurements of POPEI cores, regarding magnetic susceptibility (SI 10-5) and gamma ray attenuation (Figure 17). MS profiles are very similar between cores showing the highest values in the top half of the cores. The observable abrupt variations are related to the limits of the different cores sections.

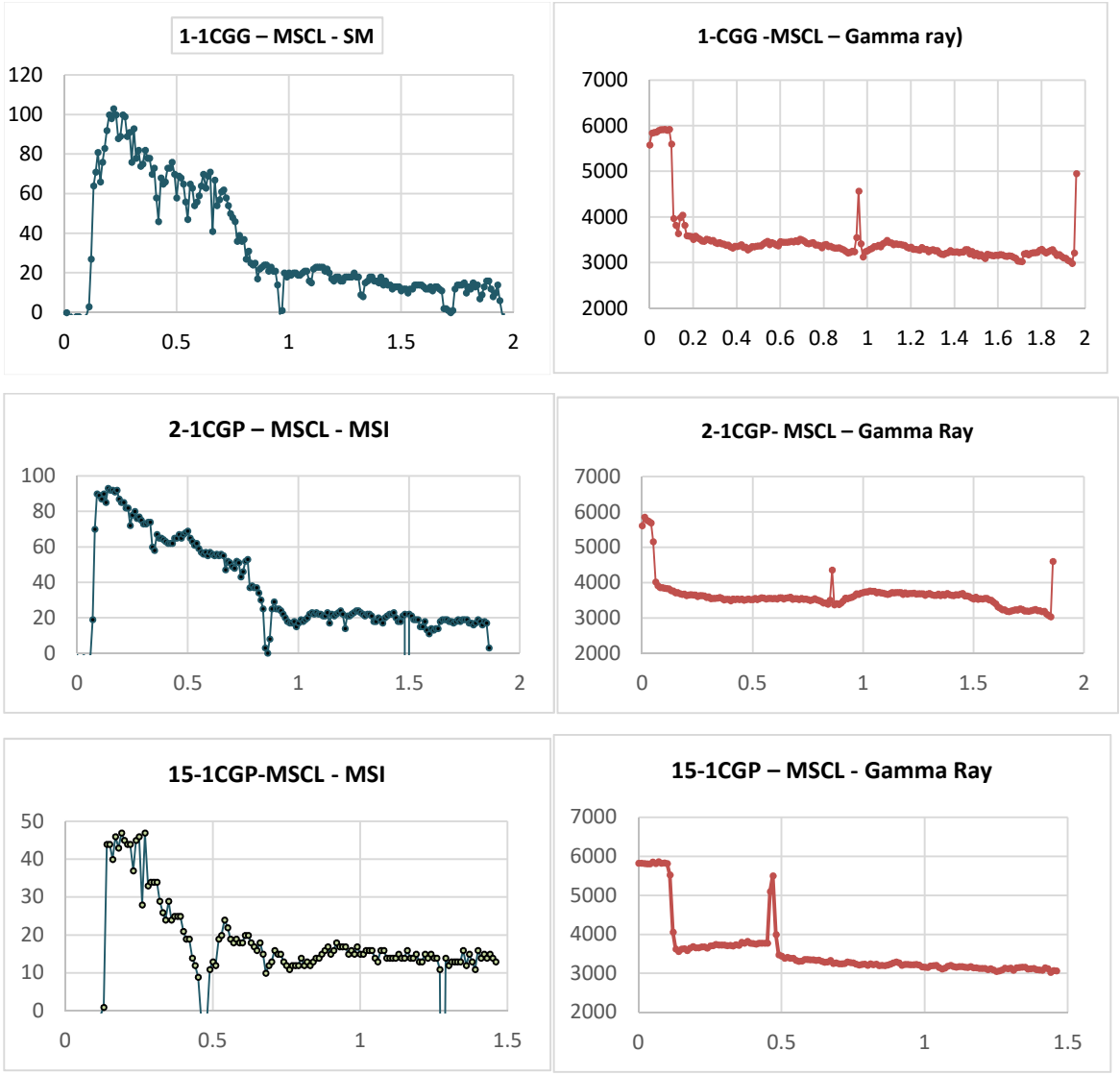

Figure 17 - POPEI cores MSCL data - Magnetic susceptibility and Gamma ray attenuation.

The magnetic susceptibility (SI 10-5) profiles of MOWER cores are very similar between them and to POPEI cores. Gamma density (gm/cc) profiles are also very similar to the mean grain size profiles (Figure 18).

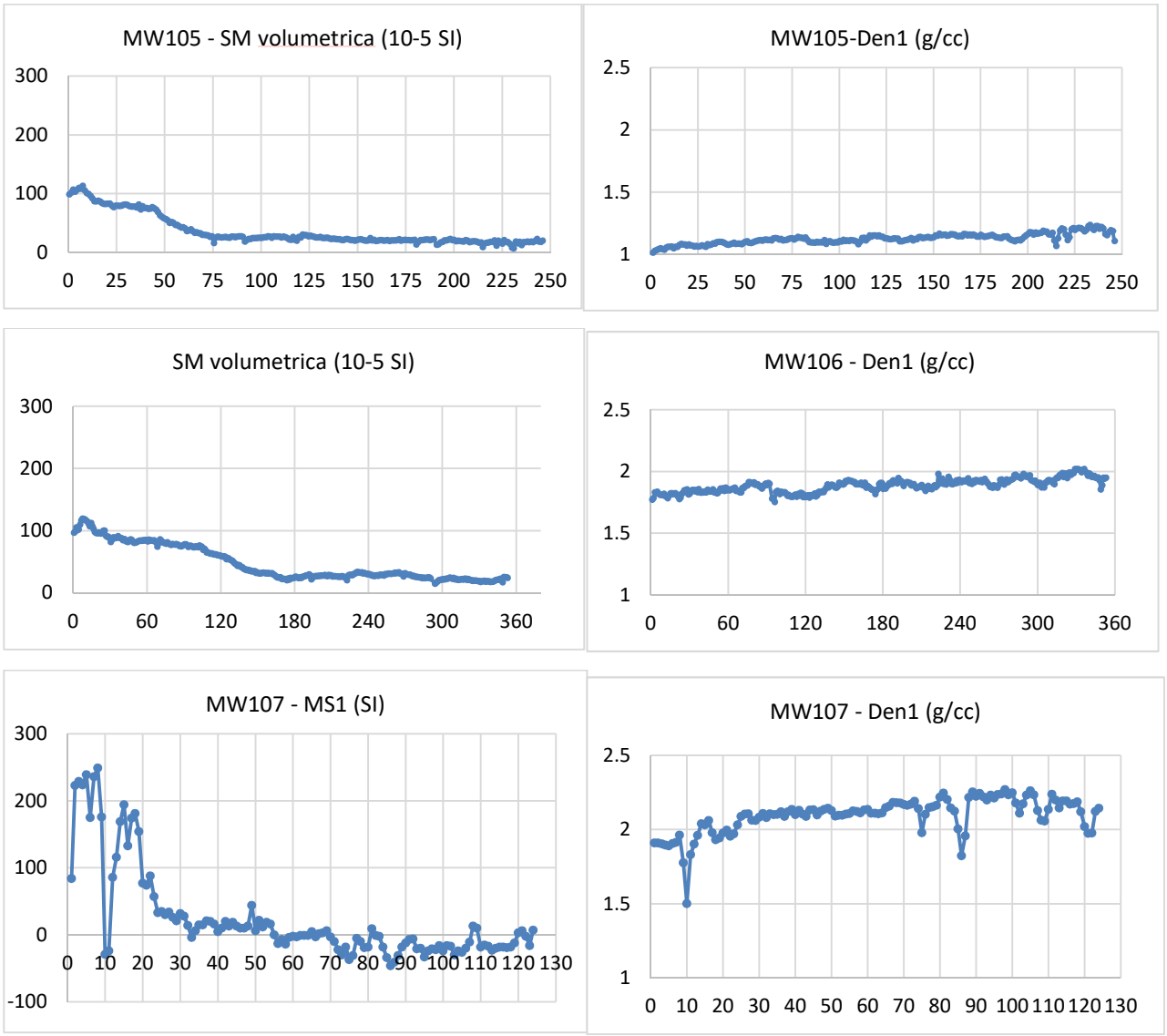

Figure 18 – MOWER cores MSCL data - Magnetic susceptibility and gamma density.

4.5. X-Ray Fluorescence data

4.5.1. POPEI cores

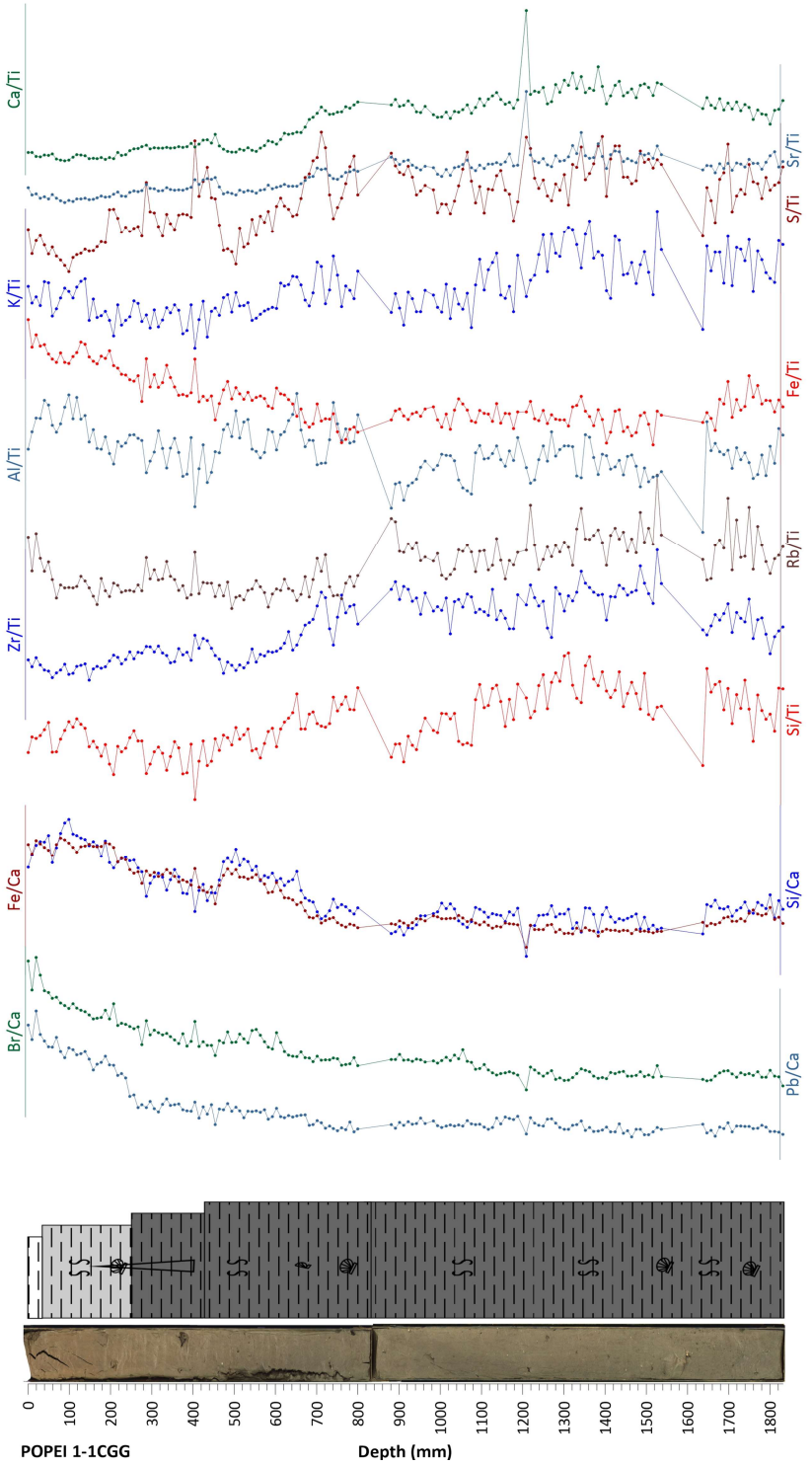

Figure 18 - POPEI 1-1CGG Ti-normalized abundance of elements used as: paleo-productivity proxies (Br/Ca and Pb/Ca); Biogenic vs Terrigenous proxies (Fe/Ca and Si/Ca); detrital source proxies (Si, Zr, Rb, Al, Fe and K); diagenetic proxies (Si, S) and; carbonate fraction proxies (Ca and Sr).

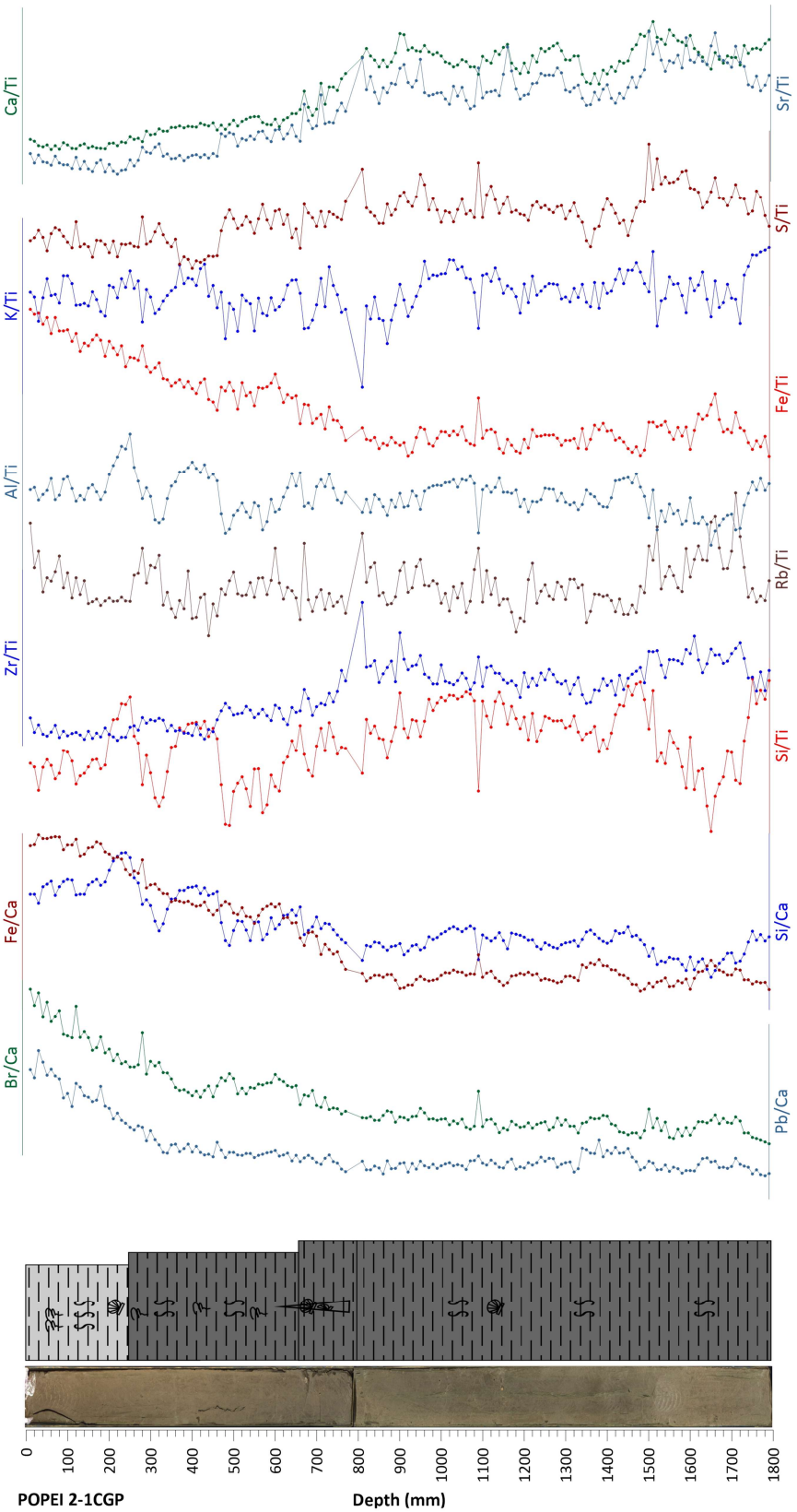

Figure 19 - POPEI 2-1CGP Ti-normalized abundance of elements used as: paleo-productivity proxies (Br/Ca and Pb/Ca); Biogenic vs Terrigenous proxies (Fe/Ca and Si/Ca); detrital source proxies (Si, Zr, Rb, Al, Fe and K); diagenetic proxies (Si, S) and; carbonate fraction proxies (Ca and Sr).

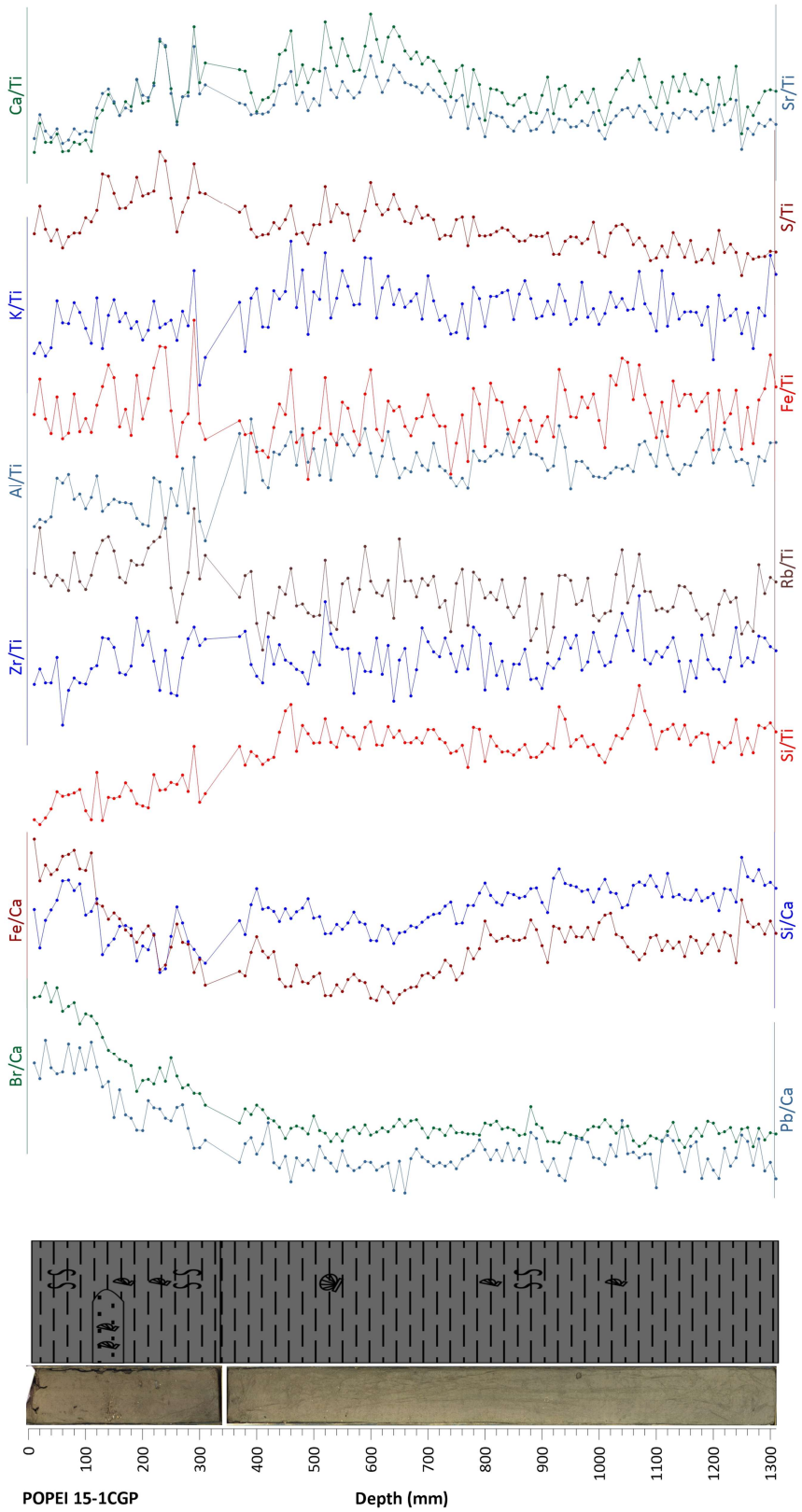

Figure 20**.** POPEI 15-1CGG Ti-normalized abundance of elements used as: paleo-productivity proxies (Br/Ca and Pb/Ca); Biogenic vs Terrigenous proxies (Fe/Ca and Si/Ca); detrital source proxies (Si, Zr, Rb, Al, Fe and K); diagenetic proxies (Si, S) and; carbonate fraction proxies (Ca and Sr).

4.5.2. MOWER cores

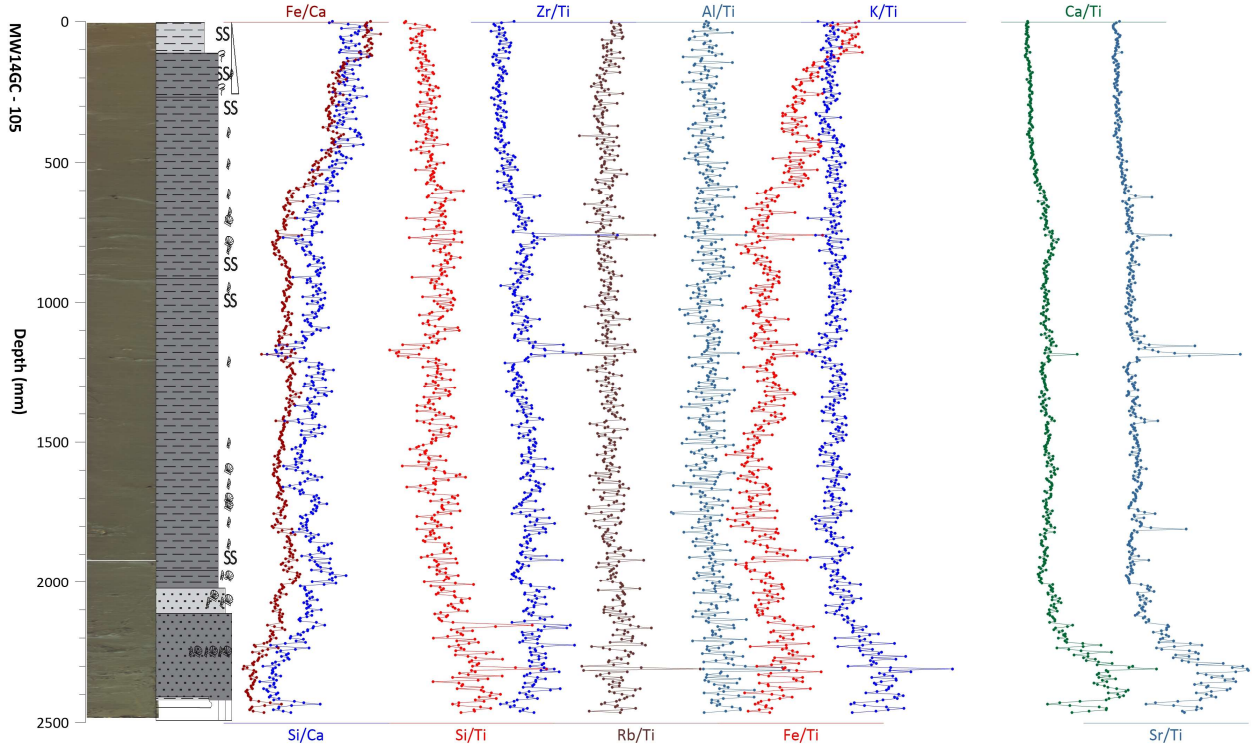

Figure 21. Mower GC 105 Ti-normalized concentrations of elements used as Biogenic vs Terrigenous proxies (Fe/Ca and Si/Ca), as detrital source proxies (Si, Zr, Rb, Al, Fe and K), and the carbonate fraction proxies (Ca and Sr).

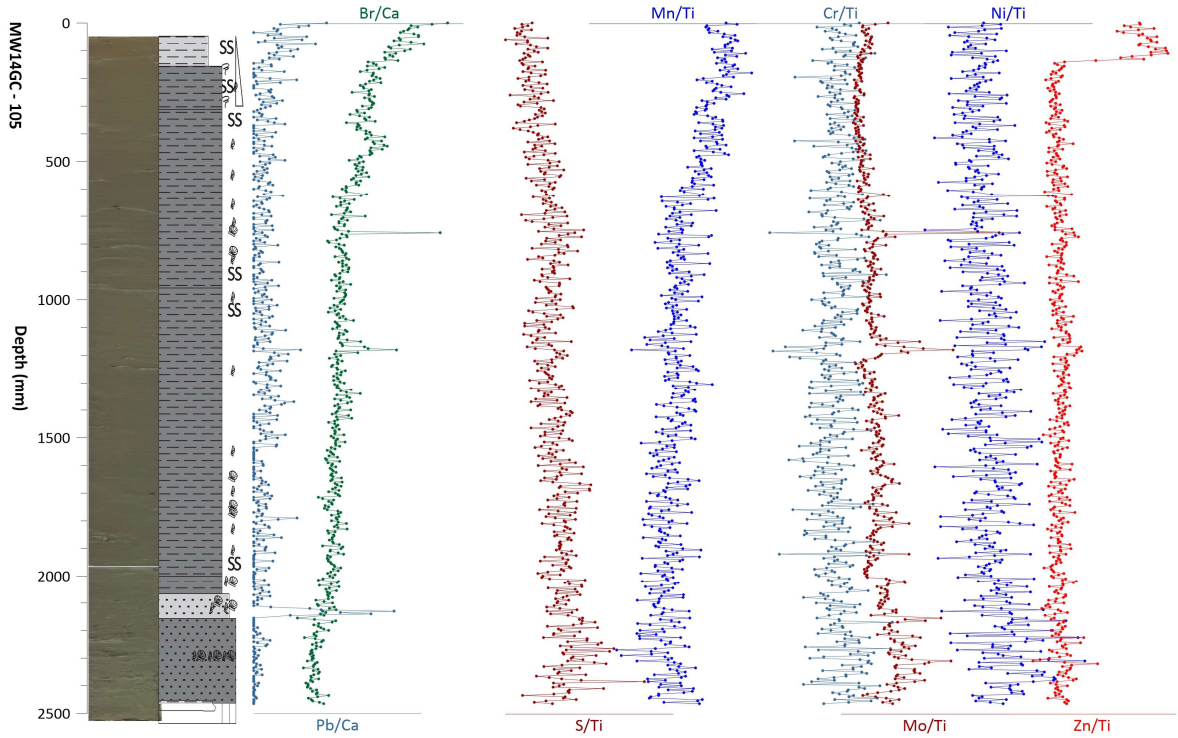

Figure 22 - Mower GC 105 Ti-normalized concentrations of elements used as paleo-productivity proxies (Br/Ca and Pb/Ca) and as diagenetic proxies (Si, Mn, Cr, Mo, Ni, and Zn).

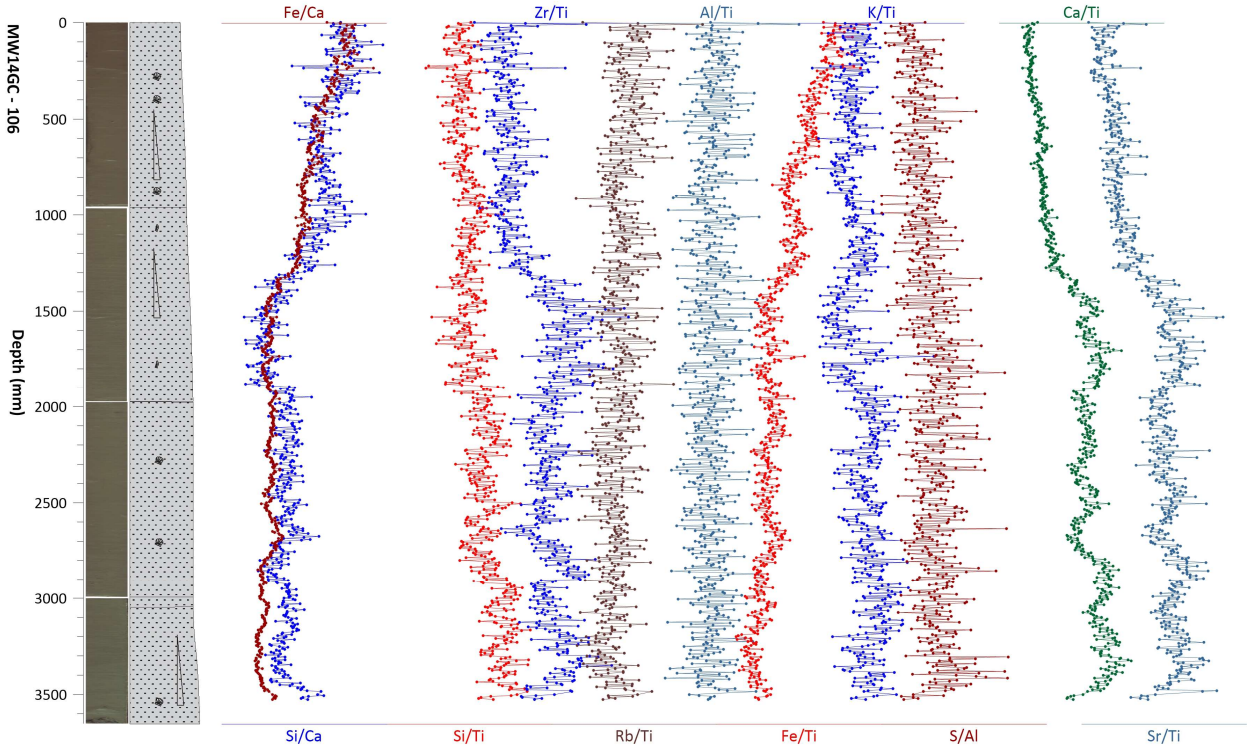

Figure 23 - Mower GC 106 Ti-normalized concentrations of elements used as Biogenic vs Terrigenous proxies (Fe/Ca and Si/Ca), as detrital source proxies (Si, Zr, Rb, Al, Fe and K), and the carbonate fraction proxies (Ca and Sr).

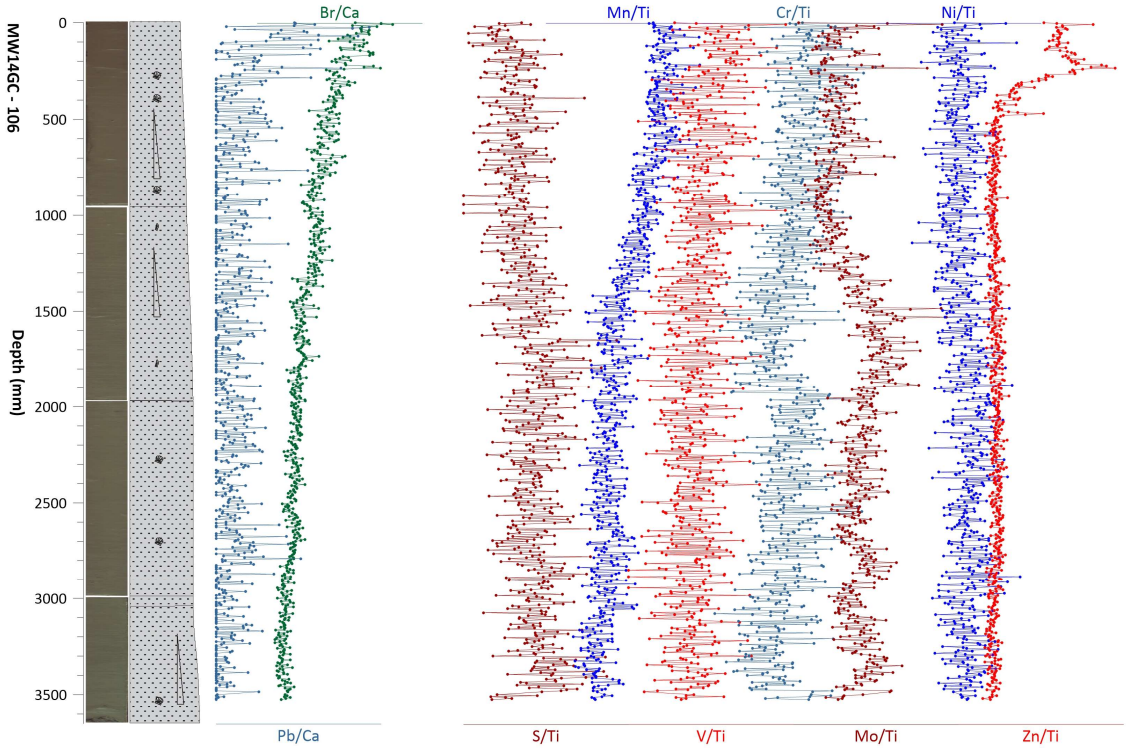

Figure 24 - Mower GC 106 Ti-normalized concentrations of elements used as paleo-productivity proxies (Br/Ca and Pb/Ca) and as diagenetic proxies (Si, Mn, Cr, Mo, Ni, and Zn).

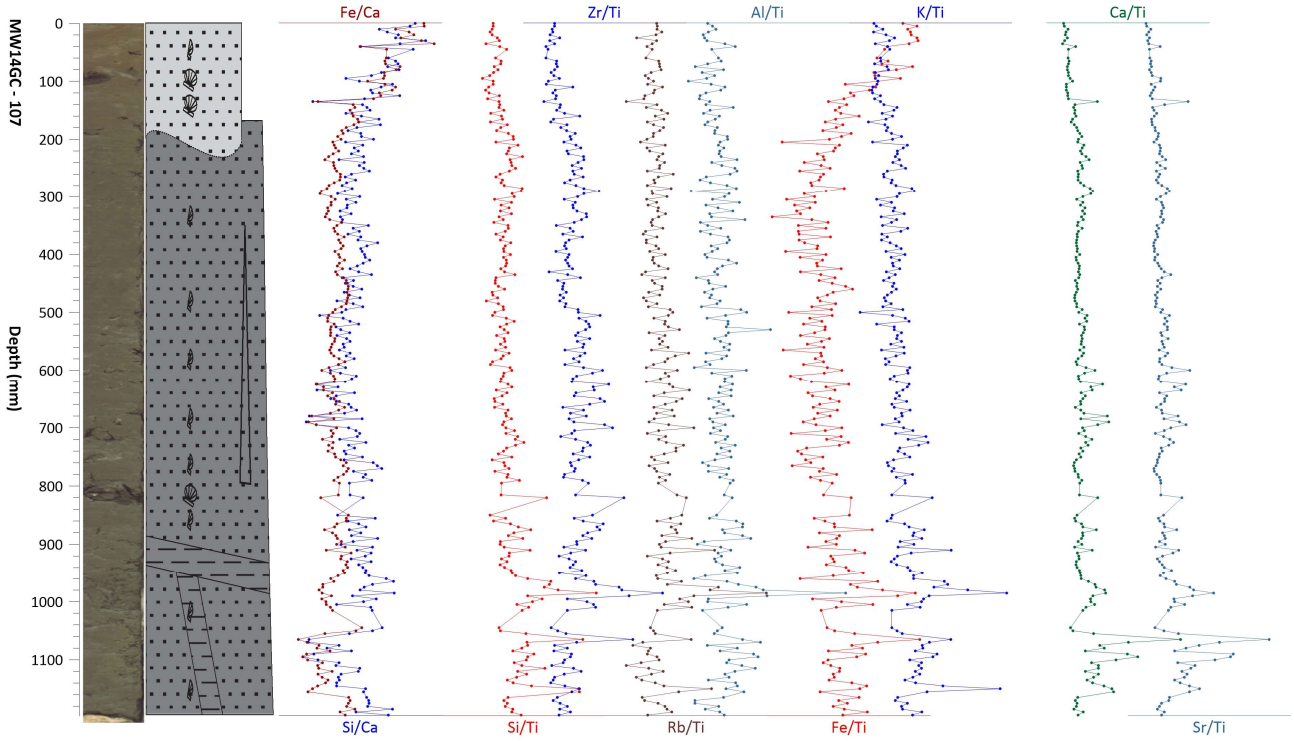

Figure 25 - Mower GC 107 Ti-normalized concentrations of elements used as Biogenic vs Terrigenous proxies (Fe/Ca and Si/Ca), as detrital source proxies (Si, Zr, Rb, Al, Fe and K), and the carbonate fraction proxies (Ca and Sr).

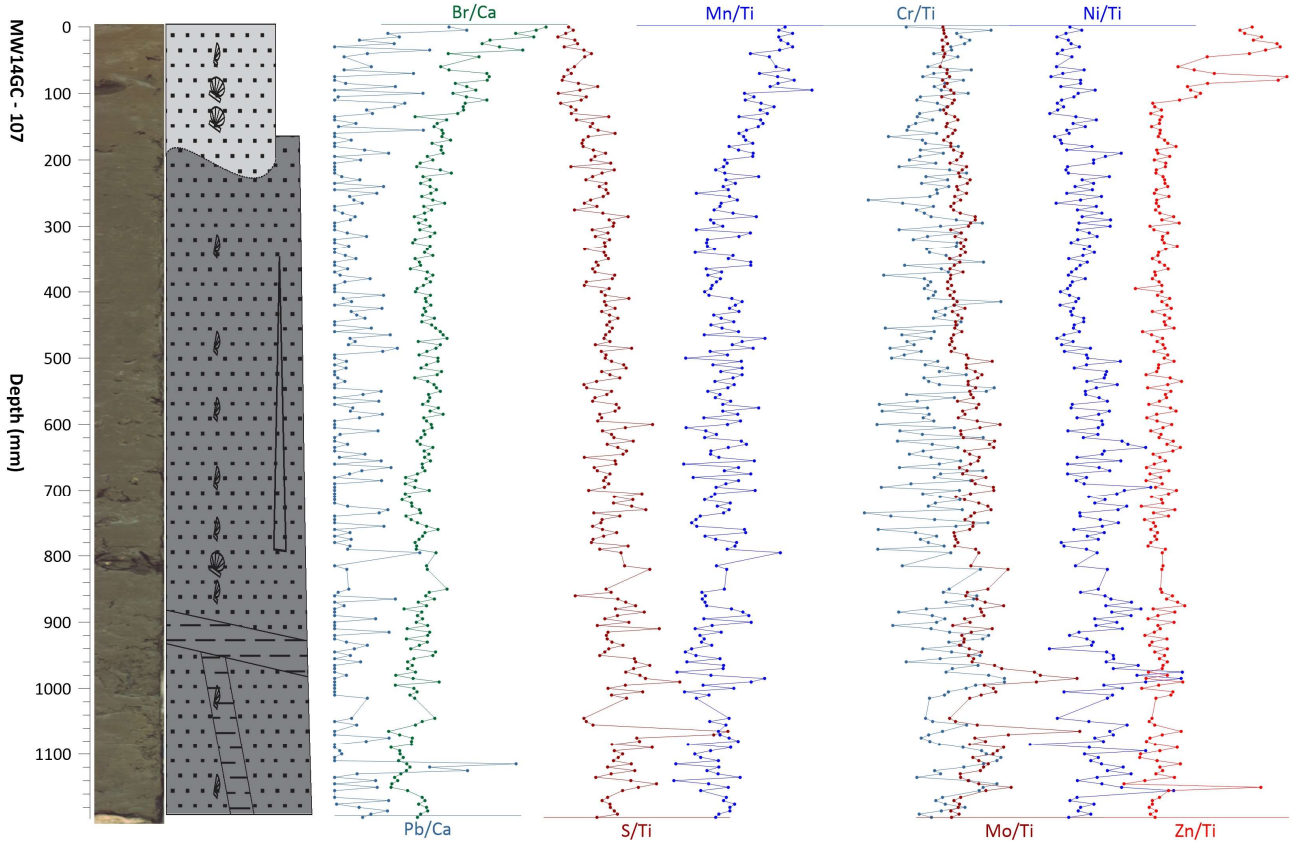

Figure 26 - Mower GC 107 Ti-normalized concentrations of elements used as paleo-productivity proxies (Br/Ca and Pb/Ca) and as diagenetic proxies (Si, Mn, Cr, Mo, Ni, and Zn).

- XRF-logs of all core show increasing Si/Ca trends from the base to the top, indicating increasing carbonated facies to the base, reflecting the increased shells content at the very coarse sand chaotic facies, also noticeable in the Ca and Sr profiles;
- Elements considered to indicate detrital source (Si, Zr, Rb, Al, Fe and K) show, in general, low variability throughout the cores, indicating a constant source of the sediments into the shelf;
- Elements considered involved in diagenetic (oxidation) processes (Mn, V, Co, S) are consistent and show increased reactivity in the top 30-40 cm;
- Pb, which is usually related with anthropogenic sources, reach higher values at the top and at very discrete layers within the very coarse sand with chaotic facies of abundant shells;
- Combined geochemical and lithological properties of the cores allowed us to define very discrete layers that represent anomalous behavior in relation to the general trends along the cores. In particular, events associated with high energy or abnormal sedimentary sources are being investigated with more detail to evaluate their potential relationship with past tsunami episodes.

4.6. AMS C^{14} and Pb^{210} dating

Pb210 contents and AMS Carbon-14 dating data are a work in progress. In the following tables, it is represented the obtained results (tables III and IV).

Table III – Results from Pb210 analysis (total and excess). Legend: SR = Sedimentation rate

	POPEI						**MOWER**					
	1-1CGG		**2-1CGP SR = 0.24 cm/y**		**15-1CGP**		**MW105 SR=0.089 cm/y**		**MW106 SR =0.28cm/y**		**MW107 SR=0.081 cm/y**	
Level (cm)	Pb210 total	Pb210 excess	Pb210 total	Pb210 excess	Pb210 total	Pb210 excess	Pb210 total	Pb210 excess	Pb210 total	Pb210 excess	Pb210 total	Pb210 excess
0.5			194	173.2			253	231.1	202	182.2	116	97.8
1.5							207	183.2				
2.5			197	176.7			107	86.0	165	143.7	123	101.6
4.5			150	127.4			78	58.4			62	40.5
7.5			138	118.6			40	18.8	112	88.6	27	8.9
10.5							29	7.1	88	63.9	23	5.0
13.5			62	41.3					80	59.4		
15.5									70	50.7		
19.5			39	15.8					38	14.8		
24.5									34	13.1		
34.5												

Table IV – Results from AMS dating.

	Submitter ID	Material Type	Conventional Age	Calibrated Age
	Beta Analytic 1-1CGG_5152	Forams	960 +/- 30 BP	Cal AD 1460 to 1820 (Cal BP 490 to 130)
POPEI 1 -1 CGG	Actalabs **1-1CGG-7879**	Shell	**1140 +/- 40 BP**	**Cal 660 - 720 AD**
	Beta Analytic 1-1CGG_113114 (113-114cm)	Shell	2130 +/- 30 BP	Cal AD 355 to 700 (Cal BP 1595 to 1250)
POPEI 2-1CGP	Beta Analytic 2-1CGP_6061 (60-61cm)	Shell	660 +/- 30 BP	Cal AD 1705 to Post 1950 (Cal BP 245 to Post 0)
	Beta Analytic 2-1CGP_8990 (89-90cm)	Shell	1240 +/- 30 BP	Cal AD 1270 to 1505 (Cal BP 680 to 445)
	Beta Analytic 2-1CGP_132133	Forams	2130 +/- 30 BP	Cal AD 355 to 700 (Cal BP 1595 to 1250)
	Beta Analytic 2-1CGP_158159	Forams	2670 +/- 30 BP	Cal BC 335 to AD 130 (Cal BP 2285 to 1820)
MOWER MW105	Beta Analytic MW105_7980	Shell	1140 +/- 30 BP	Cal AD 1320 to 1645 (Cal BP 630 to 305)
	Actalabs MW14-GC105_125126	Mix Benthic Foraminifers	2450 +/- 30 BP	Cal 750 - 680 BC (26.7%) Cal 670 - 610 BC (15.5%) Cal 600 - 410 BC (53.2%)
	Actalabs MW14-GC105_155156	Shell	3280 +/- 30 BP	Cal 1630 - 1500 BC
	Actalabs MW14-GC105_165166	Shell	3480 +/- 30 BP	Cal 1880 - 1690 BC
	Actalabs MW14-GC105_186188	Shell	4200 +/- 30 BP	Cal 2890 - 2840 BC (27.1%) Cal 2810 - 2680 BC (68.3%)
	Actalabs MW14-GC105_204206	Shell	**5350 +/- 40 BP**	**Cal 5750 - 5560 BC**
	MW14-GC105_235236	Shell	8280 +/- 30 BP	Cal 7460 - 7190 BC
	Beta Analytic	Forams		
	Beta Analytic	Forams		
	Beta Analytic	Forams		
	Beta Analytic	Forams		
	Beta Analytic	Forams		
	Beta Analytic	Forams		

	Beta Analytic			
MOWER MW106	Beta Analytic MW106_265266	Shell	2340 +/- 30 BP	Cal AD 95 to 535 (Cal BP 1855 to 1415)
	Beta Analytic MW106_318319	Shell	3120 +/- 30 BP	Cal BC 825 to 390 (Cal BP 2775 to 2340)
MOWER MW107	Actalabs MW14-GC107_2829		**1380 +/- 40 BP**	**Cal 900 - 960 AD**
	Actalabs MW14-GC107_6869	Shell	3380 +/- 30 BP	Cal 1740 - 1620 BC
	Actalabs MW14-GC107_9091	Shells + gastropods	5260 +/- 30 BP	Cal 4230 - 4200 BC (12.5%) Cal 4170 - 4090 BC (31.5%) Cal 4080 - 3980 BC (51.4%)
	Beta Analytic MW107_110111	Shell	5600 +/- 30 BP	Cal BC 3945 to 3590 (Cal BP 5895 to 5540)

5. DISCUSSION

5.1. Searching for evidences of offshore tsunamigenic deposits

While some of the data is still being processed and analyzed, the present-day data do not clearly put in evidence any clear tsunamigenic event in the offshore sedimentary record. However, based on the variations in grain-size, XRF and magnetic parameters results, we've tried to discriminate some levels defined by more or less marked grain-size analysis variations (increase or decrease in grain-size, usually expressed in the mean grain-size – Figures 4a-9a) by the increase of terrigenous proxies (Fe/Ca and Si/Ca) or detrital source proxies (Si, Zr, Rb, Al, Fe and K) (Figure 14) in XRF data and in magnetic mineral phases we've considered variations in several environmental magnetic parameters and their ratios along cores depth (Figures 18 to 25): mass normalized low field magnetic susceptibility, IRM - isothermal remanent magnetization; susceptibility of anhysteretic remanent magnetization; S-Ratios acquired by back fields of 100 mT ($SR_{0.1}$) and 300 mT ($SR_{0.3}$) after application of a direct field with 1000 mT χ_{FD} (%) magnetic susceptibility frequency dependence.

The selected levels are represented in the following table (Table V) and we prefer called them "anomalous levels". Those may correspond to high energy events, with characteristics that we would expect from tsunamigenic events. Those that are coincident in the three proxies (Sedimentology, XRF and Magnetism) are represented in dark blue color (Table V). Based on the available Pb210 and C14 data we've tried to date the selected levels and interestingly, in the most cores (all the Mower cores and in the 2-1CGP POPEI core), the AD 1755 event seems to be represented.

Table V – Table synthesis of "anomalous levels" based on sedimentological data (Sed), XRF and magnetic parameters (Mag). Legend: bsf – bottom of sea floor; TBD – to be determined; SR – sedimentation rate. Evidences for the chosen levels can be observed in the discriminated figures and those represented in the three proxies (sed, XRF, Mag) are evidenced in dark blue colors; √ - event confirmed;? – Event not clear.

Event number	Core/seismic line	Depth bsf (cm)	Sed	XRF	Mag	EstimatedAge	Observations/Figures
1	**POPEI 1–1CGG** Water depth: 76 m Length: 1.84 m	20-25	√	√	√	TBD	-------- Figs.4a, 14 and 18
2		45-50	√	√	√	TBD	-------- Figs.4a, 14 and 18
3		100-108	√	√	?	<355-700 AD	14C calibrated at 113-114 cm Figs Fig.4a, 14
4	**POPEI 2–1 CGP** Water depth: 84.45 m Length: 1.80 m	60-70	√	--	√	1705 -1950 AD	14C calibrated at 60-61 cm Event 1755. Figs.5a and 14
5		80-90	√	--	√	1270-1505 AD	14C calibrated at 89-90 cm Figs.5a and 14
6		130-140	√	√	?	TBD	-------- Figs.5a and 19
7		155-160	√	√	--	TBD	-------- Figs.5a and 19
8	**POPEI-15** Water depth: 87.14 m Length: 1.41 m	20-26	√	√	√	TBD	-------- Fig.6c,6d, 14 and 20
9		65-70	√	√	√	TBD	-------- Fig.6c, 6d, 14 and 20
10		85-90	√	--	√	TBD	-------- Fig.6a and 14
11	**MW14-105** Water depth: 77.11 m Length: 2.50 m	20-25	--	--	√	1733-1789 AD	Estimated based on 210Pb data (SR) Event 1755 Fig. 14
12		38-44	√	√	√	1520-1578 AD	Estimated based on 210Pb (SR) Fig.7a, 14 and 21
13		76-84	√	√	√	1320-1645 AD	14C calibrated at 79-80 cm Fig.7a, 14 and 21
14		116-224	--	√	--	<600-410 BC	14C calibrated at 125-126 cm Fig.21
15		160-190	√	--	√	1880-2680 BC	14C calibrated at 165-166 cm and 186-188 cm Figs.7a and 14
16		210-240	√	√	√	**Cal 5750 - 5560 BC** 7460-7190 BC	14C calibrated at 204-205cm 235-236 cm Fig.7a, 14 and 21
17	**MW14-106** Water depth: 90.81 m Length: 3.53 m	62-70	√	√	√	1793-1764 AD	Event 1755 Estimated based on 210Pb data (SR) Fig.8a, 14 and 23
18		83-90	√	--	√	TBD	-------- Fig.8a and 14
19		130-140	√	√	--	TBD	-------- Fig.8a and 23
20		175-195	√	√	√	TBD	-------- Fig.8a, 14 and 23
21		260-273	√	√	√	95-535 AD	14C calibrated at 265-266 cm Fig.8a, 14 and 23
22		320-330	√	√	√	825-390 BC	14C calibrated at 318-31 cm Fig.8a, 14 and 23
23	**MW14-107** Water depth: 56.76 m Length: 1.25 m	18-22	√	--	√	1792-1742 AD	Estimated based on 210Pb data (SR) Event 1755, Figs.9a and 14
24		30-35	√	√	?	1644-1582 AD	Estimated based on 210Pb data (SR) Fig.9a and 25
25		67-72	√	√	√	1740-1620 BC	14C calibrated at 68-69 cm Fig.9a, 14 and 25
26		103-122	√	√	√	3945-3590 BC	14C calibrated at 110-111 cm Fig.9a, 14 and 25

II. Results from the acquisition and study of offshore seismic reflection seismics

1.INTRODUCTION

The coast of the Algarve, south Portugal, was severely struck by the 1755 Great Lisbon earthquake and tsunami and a series of tsunami deposits have been reported (references). Other tsunamis have also been reported to have struck the Algarve coast in the past. Various high energy deposits have been described onshore near Algarve, across the Portugal-Spain border.

Identification, dating and mapping of offshore high energy deposits, i.e. sedimentation events deposited under hydrodynamic conditions regardless of their origin, was considered as a first step towards the understanding of past tsunami events. Hopefully, a comprehensive description of these deposits will, in the future, allow for better classification and ascribe deposits with their origin, such as storms, tsunamis, landslides etc.

With this final goal in mind, high and ultra-high resolution multichannel reflection seismics were used to image Mass Transport Deposits (MTDs) in the study area. i.e. offshore SW Iberia.

With the main scientific goal of finding MTDs off the Portuguese coast three potential areas of occurrence were selected for inspection, i) the deep seated Hirondelle seamount off SW Portugal, ii) the Tagus river submarine delta and iii) the Faro MTDs on the continental shelf off Algarve.

2. MTDS FROM SEISMIC REFLECTION PROFILES

2.1 The Hirondelle seamount

The South Hirondelle Seamount landslide is a slid body on the southern flank of the Hirondelle seamount (Figure 27) (Omira et al., 2016 in the scope of ASTARTE). According to these authors the landslide with estimated Quaternary age, possibly a Late Pleistocene (Figures 28 and 29), from stratigraphic correlation using Hayward et al (1999) calibration and seismic reflection profiles can have generated a tsunami on the coasts of Portugal and Morocco with maximum wave amplitudes up to >5m (Figure 30).

The main descriptive parameters have been inserted on the ASTARTE MTD database, as follows, Deposit Minimum Depth: -3290 m, Deposit Maximum Depth: -4850 m, Runout: 80 km, Area: 1200km2, Thickness: 1960 m, Scar Minimum Depth: -2240 m and Scar Maximum Depth: -3290 m.

The Hirondelle seamount is one of the seamounts of the prominent Josephine-Gorringe ridge that concentrates seismicity along the Eurasia-Africa plate boundary in the North East Atlantic.

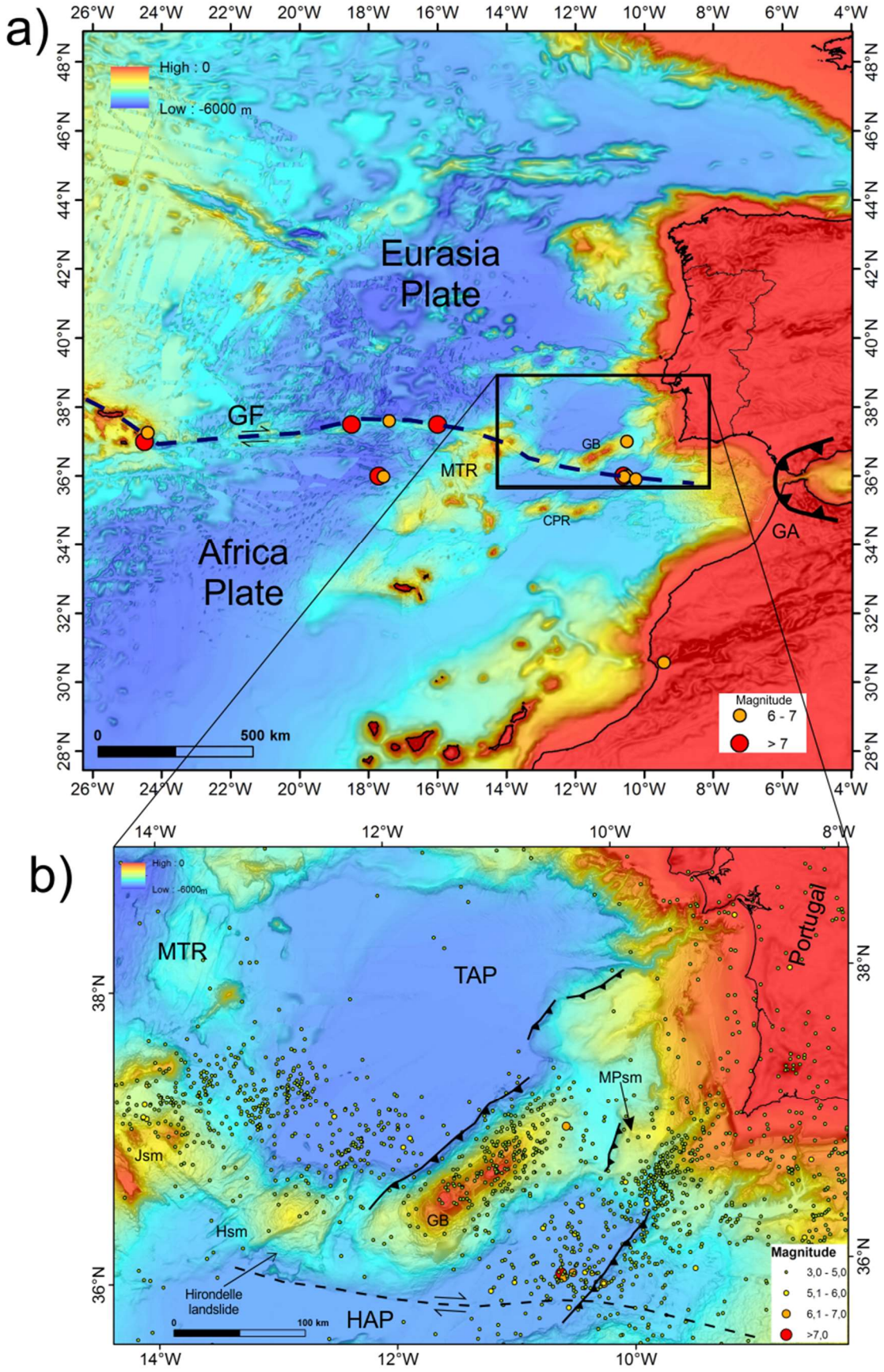

Figure 27 - Geotectonic setting of the Hirondelle seamount on the Gloria Fault-Gibraltar plate boundary. A) General location with large magnitude epicenters location; B) seismicity of the SW Iberia region and location of the Hirondelle seamount (from Omira et al., 2016).

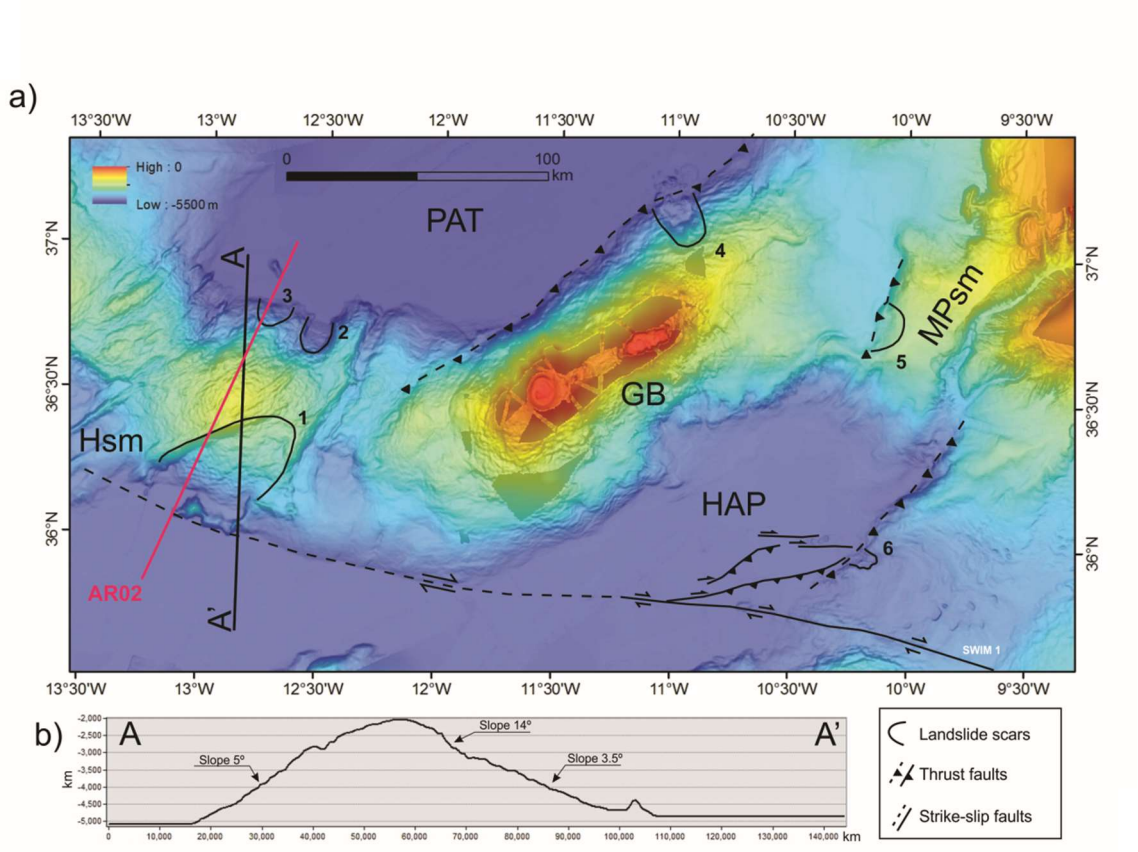

Figure 28- Morphology, structural and stratigraphic interpretation. A) Multibeam bathymetry with outline of main landslide scars (1, 2 and 3) and tectonic features. B) AA', bathymetric profile (from Omira et al., 2016).

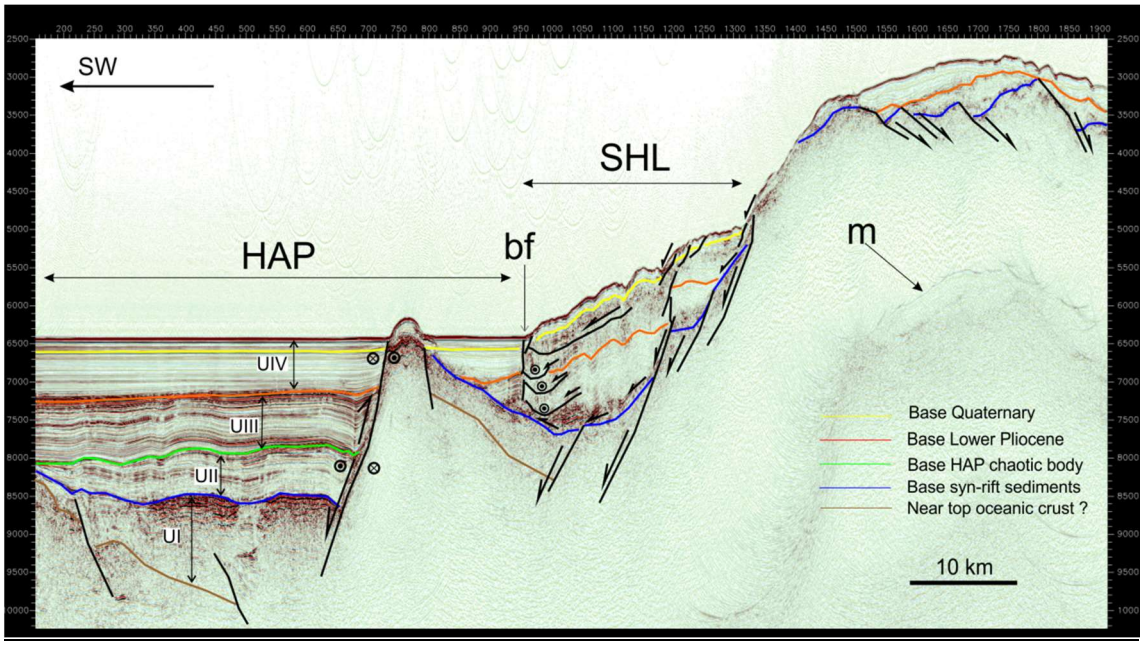

Figure 29 - Stratigraphic and tectonic interpretation of the south Hirondelle landslide (from Omira et al., 2016).

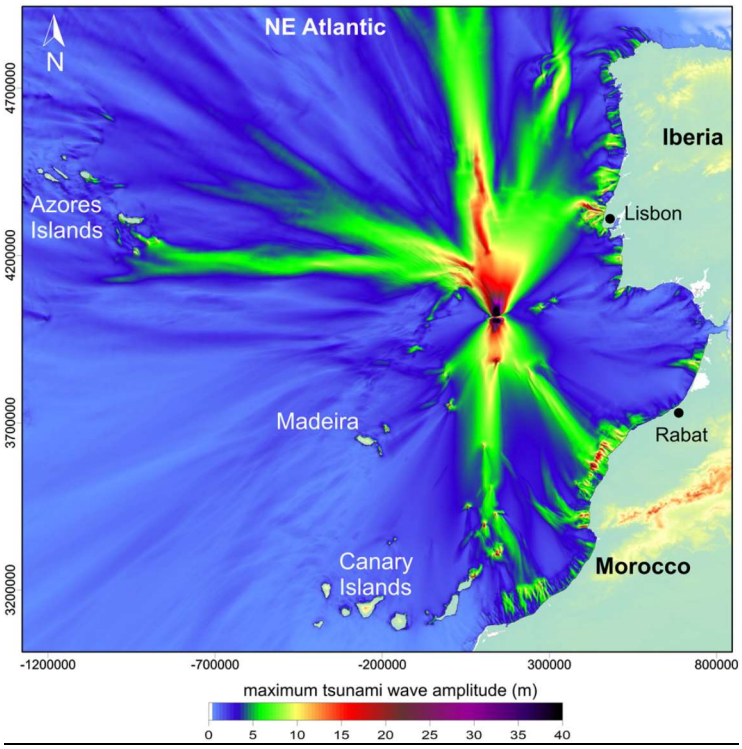

Figure 30 - Tsunami maximum wave amplitudes distribution in the NE Atlantic region due to the occurrence of the South Hirondelle submarine landslide. The map coordinates system is UTM– Zone 29 N, DatumWGS-84 (from Omira et al., 2016).

2.2 The Tagus delta landslide

The Tagus river mouth is located off Lisbon with coordinates, 38º38'N; 9º20W. The Tagus river ebb-delta depicts a crescent shape to the west of the estuary inlet, it has an estimated volume of 4 km3 to 5.5 km3, with a maximum sediment thickness of about 50 m and mean surface dimensions of approximately 13 km long - across shore - by 15 km wide - along shore (Terrinha et al., 2015).

Interpretation of high resolution seismic reflection profiles acquired during previous projects was done in the scope of the ASTARTE project. Various landslides were recognized in this dataset (Figure 31).

A submarine landslide with estimated age just over 8 ky BP from stratigraphic correlation using core D13902 from www.pangaea.de Abrantes et al. (2005; 2008) and Alt-Epping et al. (2009). The landslide is topped by the 8ky BP stratigraphic horizon. The landslide lies within a deltaic unit with its base at 13ky BP estimated age.

The main parameters were uploaded on the ASTARTE MTD database, as follows: MTD thickness: 20m max.; Volume: 0.24km3=2.4 x 108m3, Mean slope: 1º and Calendar age: 8.002 ky BP based on seismic stratigraphic correlation with 14C dating on cores by Abrantes et al. (2005; 2008).

An older group of landslides has been recognized using the same dataset. These lie within an older sedimentary unit comprised between seismic horizons of the Tagus delta speculative age, between 13ky-17ky (Figure 31). These ages must not bear a large error because they correlate with cores reported by Abrantes et al. (2005; 2008) and fit well with post Last Glacial Maximum mean sea level heights.

Various small scale MTDs above the main ~8ky event can be observe in the seismic profiles, one of which constitutes a landslide with more than one kilometer of width.

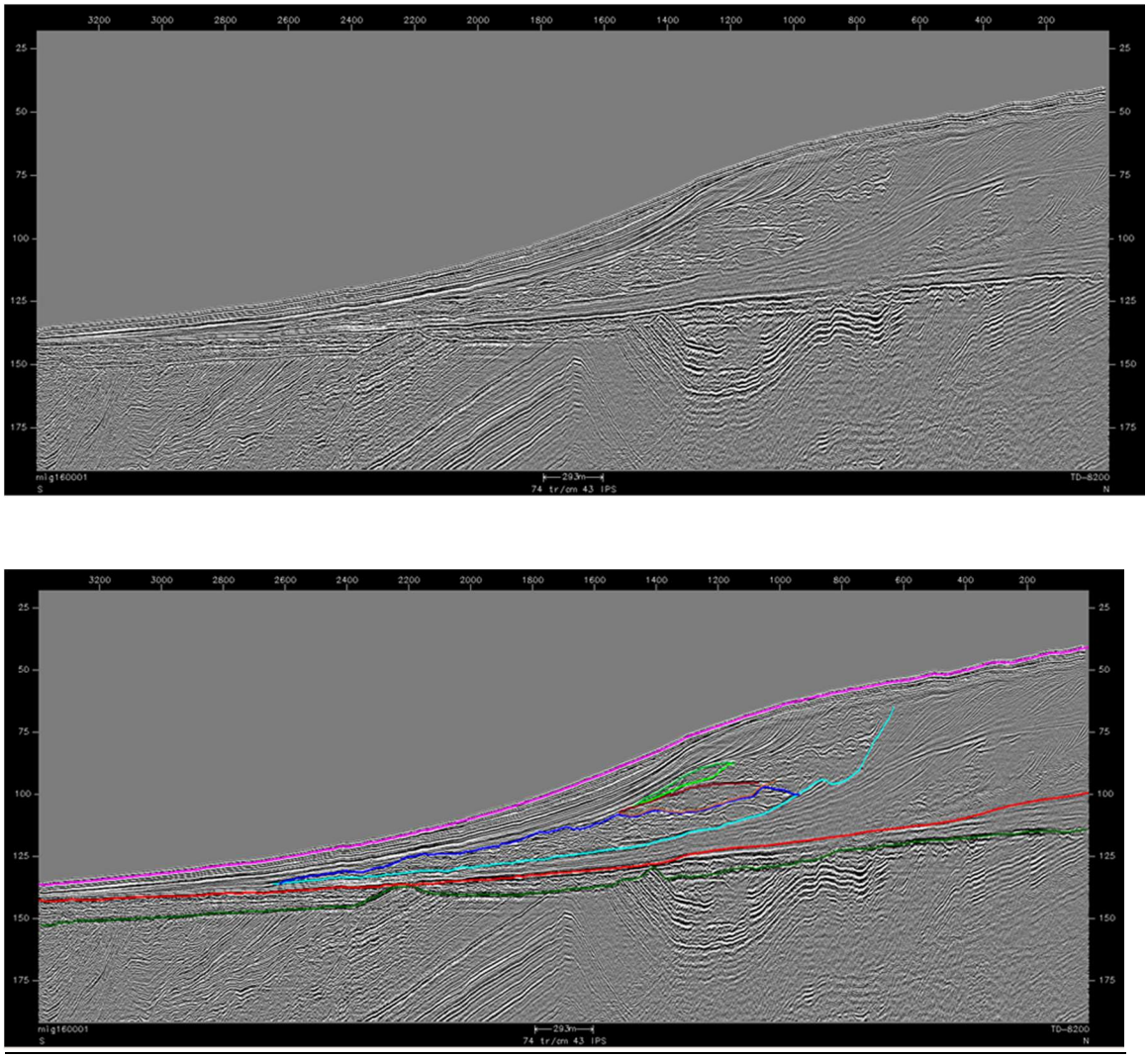

Figure 31 - The Tagus ebb-delta landslide as imaged in a high resolution multichannel seismic profile. The folded strata are Cretaceous through Pliocene in age. The seismic unit between unconformities is of Late Pleistocene age, probably redeposited during various eustatic cycles. The upper unit is the Tagus delta that contains the chaotic facies of the landslide (blue, brown and green). The total length is ~4.5km.

2.3 The Algarve MTDs

The ASTARTE 2014 high resolution multichannel seismic campaign was carried out to search for and map tsunami deposits and/or erosion structures caused by tsunamis in the continental shelf sedimentary record off Quarteira-Tavira in the Algarve continental shelf, south Portugal.

The study area comprehends the continental shelf off Quarteira (Figure 32). Gravity and vibro cores were acquired during the POPEI project in this area and were studied during ASTARTE for finding high energy or possible deposits of tsunamigenic origin. Recent work on the POPEI-2 vibrocore (Silva & Drago et al, 2012) has already reported the existence of a backwash tsunami deposit caused by the 1755 Lisbon earthquake and tsunami. Two more deposits sampled in this core are under study. The longest of the POPEI cores is 499 cm long with a maximum bottom age of ~8ky BP (vibrocorer VC2B in Mil-Homens et al. (2016).

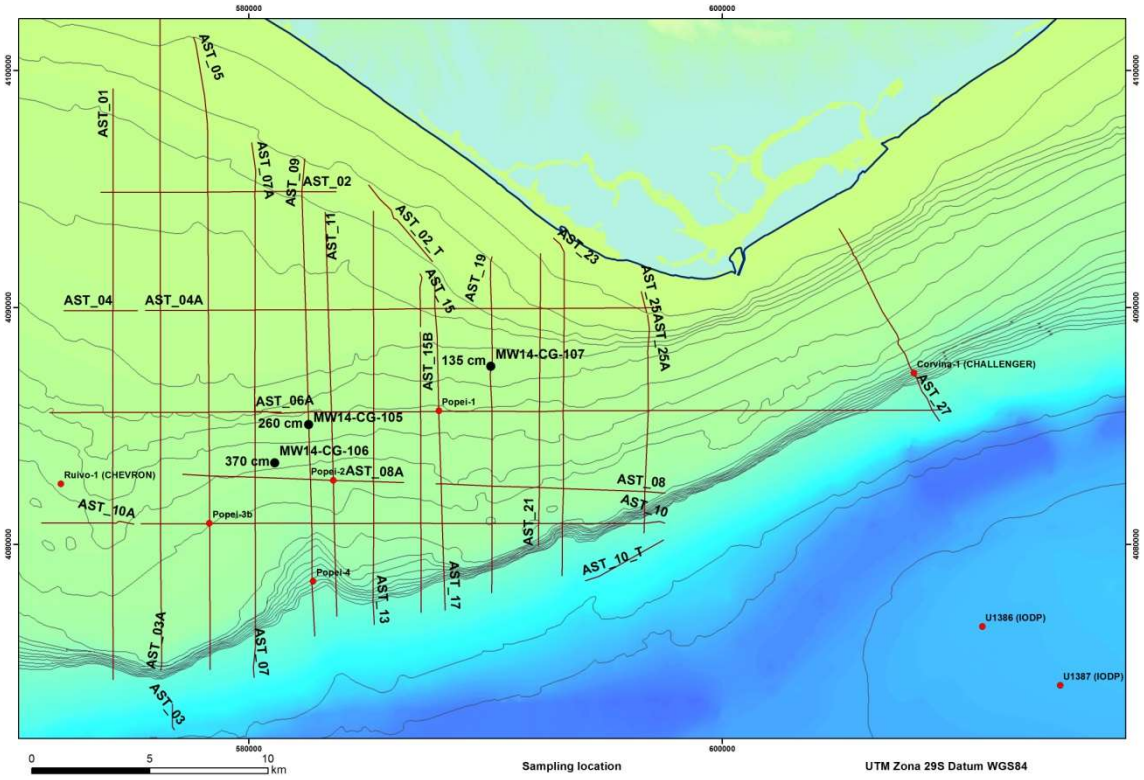

Figure 32 - Map of the ASTARTE ultra-high resolution multichannel seismic survey and location of the POPEI and MOWER cores.

The total length of acquired seismic profiles during the ASTARTE 2014 seismic survey was 320km using a Geo-Spark 1000 1kJ Pulsed Power Supply (PPS) unit with a Geo-Source 200 Light Weight Marine Multi-Tip Sparker and a 75 m Geo-Sense Light-weight 24 Channel Ultra High Resolution Streamer (UHRS) with group interval of 3,125 m.

The processing and interpretation focused on the Late Quaternary depositional units. The depositional architecture consists of a succession of progradational wedges interpreted as forced regressive wedges (seismic unit FRW). This unit is truncated by a widespread erosional surface, the transgressive surface (ST). Two lobate bodies overlay the ST, showing diverse internal acoustic facies, varying from stratified to oblique, with some sector showing chaotic facies (cf in Figure 33) at the foot of an erosional scarp. These bodies are considered transgressive deposits (seismic unit TD) according to their geometry and facies. Calibration with the core POPEI 2 allowed assigning an ^{14}C calibrated age of 8562 years AD to sediments at top of the green horizon (Figure 34). The transgressive deposits are covered by highstand aggradational or progradational deposits (seismic unit HD). The main findings regarding the presence of MTDs of certain Holocene age deposits are associated with a transgressive multi-cyclic deposits (seismic units TD) and minor events within the high-stand deposits (seismic unit HD) (Figures 35 and 36).

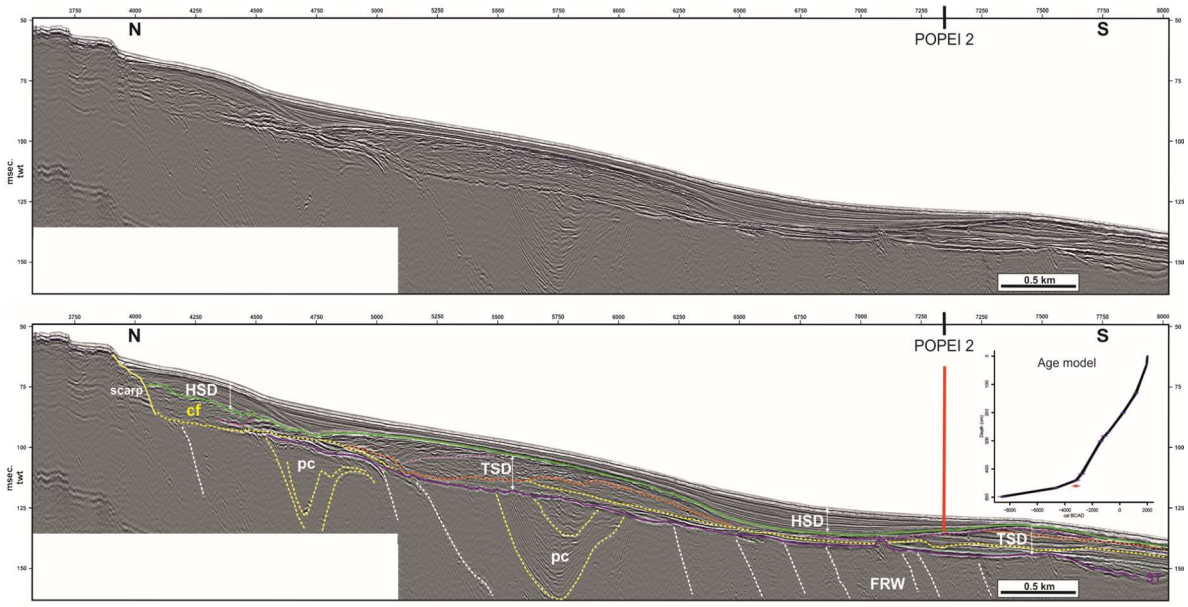

Figure 33a- Seimic line ASTARTE 11 (top) with location of core POPEI 2BVC and interpretation (bottom). FRW, forced regressive wedges; Pc, paleochannels; TS, transgressive surface; TD, transgressive deposit; HD, highstand deposit; cf, chaotic facies. Stratigraphic calibration of the line was made using the age model by Mil-Homens et a. (2016).

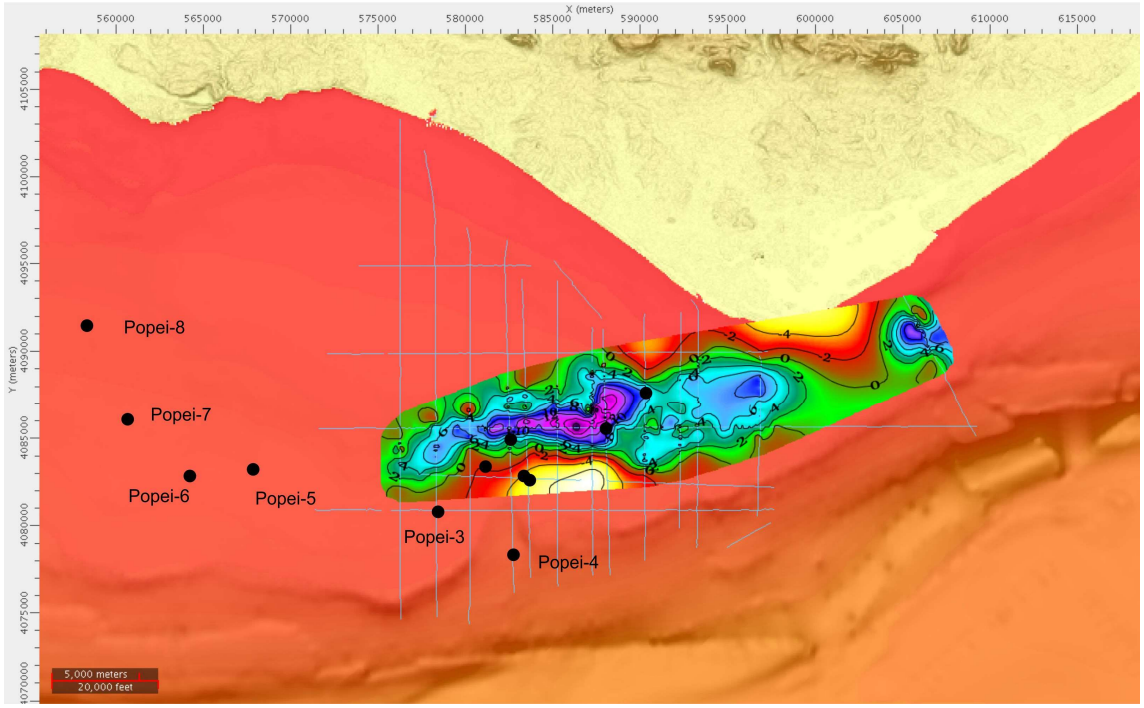

Figure 33b- Isopach map of the transgressive body (TB) shown in figure 33a. The lateral extension of the TB exceeds 20km using the ASTARTE seismic coverage. The MTDs lie inside this body have thus regional significance. Maximum thickness of the TB is 16msec, approximately 16m.

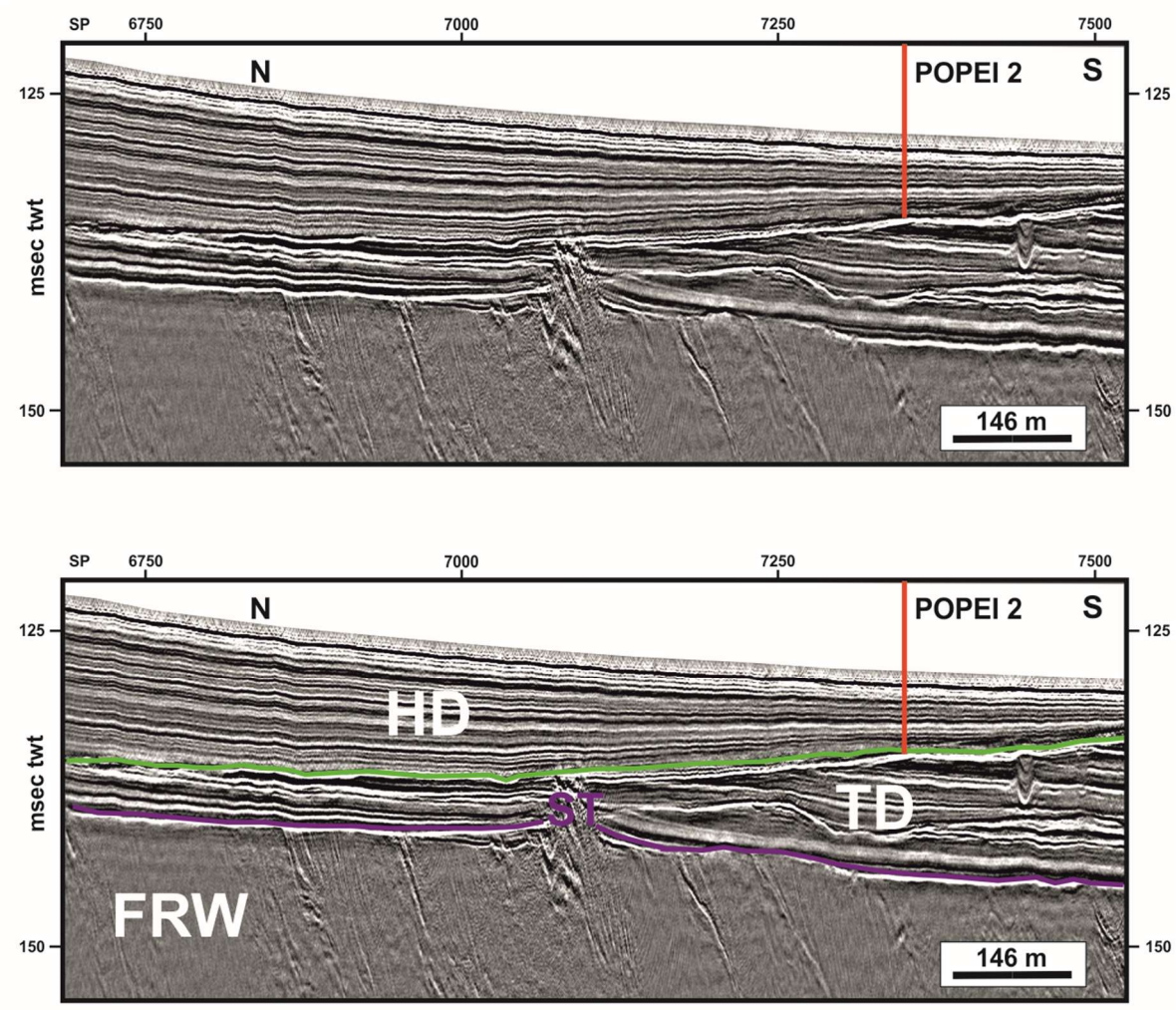

Figure 34 - Detail of seismic line ASTARTE 11 showing the stratigraphic calibration with core POPEI 2 BVC. The 14C calibrated age (Mil-Homens et al. (2016)) oldest sediments near the top of the transgressive body TD is 8562 y BP; FRW, forced regressive wedges; DH, highstand deposits; TS- transgressive surface.

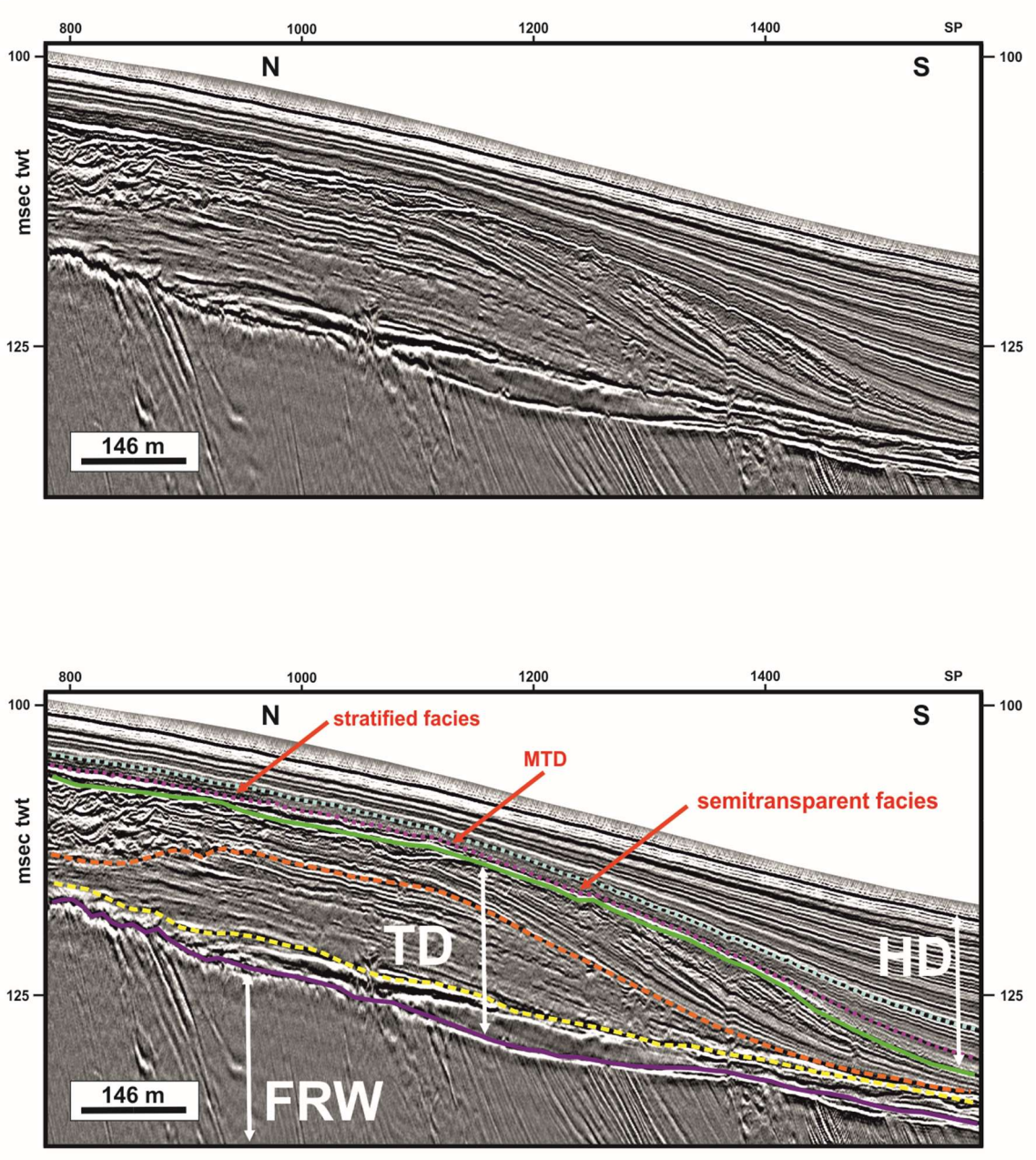

Figure 35 - Seismic profile ASTARTE 09 showing an interpreted MTD covering the transgressive body and within the highstand deposition unit (HD). The MTD body shows a clear lateral acoustic facies change from well layred to semi-transparent. FRW. Forced regressive wedge.

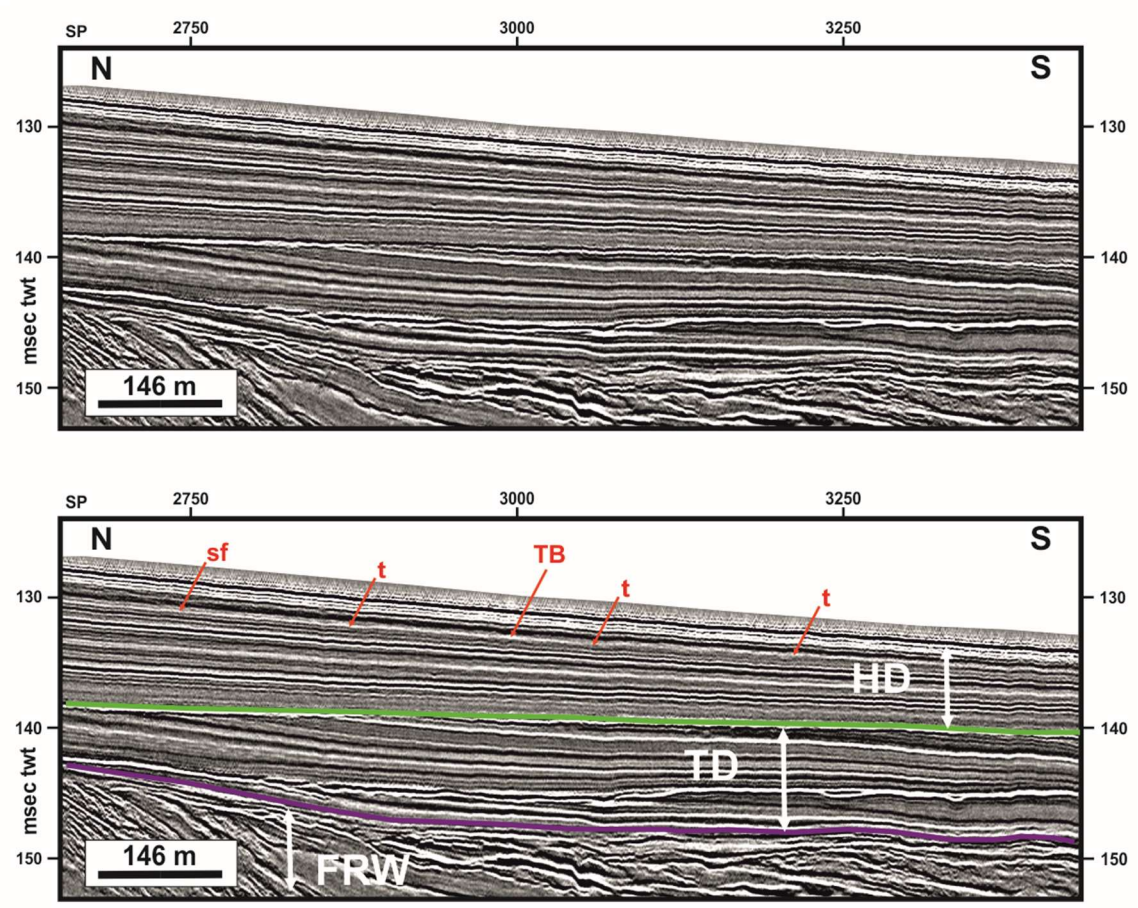

Figure 36 - Segment of ASTARTE 07 seismic profile showing the detail of an interpreted MTD based on the transparent facies cutting down well layered deposits. Thickness of the transparent layer is 0.75millisec TWT; 0.56m, vertical resolved layers indicate resolution of 0.15m. The downslope MTD shown in this seismic profile correlates with anomalous layers at 130-140cm core MW14-106 located upslope (figure 35). This seismic-core analysis correlation reinforces the probable MTD significance of the anomalous layers interpreted from core data only.

III. FINAL CONSIDERATIONS

THE ALGARVE COAST

The sedimentary record studied in this work provided information that goes back 9ky. The multidisciplinary work here conducted reveals the presence of several levels where the sedimentation regime is disturbed, mostly characterized by an increase of terrigenous inputs, as revealed by magnetic, sedimentological and XRF analyses.

Based on these proxies 26 anomalous levels were identified, 13 of which have anomalies of all three proxies (Sed, XRF, mag).

Some of these anomalous levels occur in all the cores as they yielded the same ^{210}Pb or ^{14}C age interval suggesting a common geologic process on their origin.

In 4 gravity cores an anomalous level with an age interval comprehending 1755 AD (the age of the Lisbon earthquake and tsunami) was identified, thus suggesting that these anomalous levels correspond to a high energy event associated with the 1755 tsunami.

Three anomalous levels identified in MW14-105 and MW14-106 match with MTDs described on the ultra-high seismic profiles in the Algarve continental shelf, suggesting that the geologic events associated to the deposition of these levels affected a significant area of the shelf.

A complex transgressive body between 8.64ky and 6ky AD containing MTDs with a minimum surface of 20x4 km was also mapped. The internal complexity of this body bounded by a coastal escarpment suggests a complex geological depositional history controlled by sea level changes. This indicates that MTDs in the Algarve shelf are associated not only with seismicity alone but also with eustatism and coastal dynamics.

Comparison of the ages of the here identified anomalous levels match ages of high-energy events reported from lowlands deposits in SW Spain by Luque et al. (2002) and Ruiz et al. (2005) between 300y BC and 3089y BC. This may indicate a large scale of the involved high-energy process encompassing onshore-offshore areas.

Further dating of some of the anomalous levels is awaited and it is hoped that they will allow further correlation of events.

This work represents the first systematic high resolution study on sedimentary record in the S and SW Portuguese continental shelf in the search for MTDs including backwash tsunami evidences. Our results indicate that this shelf is a suitable recorder of high-energy/tsunamigenic deposits.

THE TAGUS RIVER

The Landslides found in the Tagus river ebb-delta were deposited in shallow than today's submarine conditions. The size of the only one mappable landslide (~10kmx4kmx20m) with ~8kyBP, the existence of older ones of probable 13-17ky BP of age and a set of landslides and MTDs with less than 8ky BP constitute an indication that the delta is unstable at a timescale of various thousand years.

Since the delta is a shallow water body (20 to 100 meters below present day sea level) and is located nearby the Lisbon city, landsliding in this area is prone to cause tsunamis on the nearby coast.

THE SOUTH HIRONDELLE LANDSLIDE

Mapping and numerical model strongly indicate that a landslide with ~500 km^3 of volume has generated a tsunami on the NW and SW coasts of Morocco and Iberia, respectively.

IV. OUTREACH

- Lopes, A., P.F. Silva, T. Drago, V. Magalhães, C. Roque, A.I.Rodrigues, A. Kopf, D. Völker, P. Terrinha & M.A. Baptista (2015) - Magnetic parameters and their contribution to the identification of tsunami levels

in the sedimentary record off Algarve (South of Portugal) - Preliminary results. pp. VIII Symposium on the Iberian Atlantic Margin Proceedings, 401-404.

- Duarte D., Santos J., Terrinha P., Brito P., Noiva J., Ribeiro C. and Roque C. (2017). High resolution seismic stratigraphy and Mass Transport Deposits of the proximal continental margin, offshore Quarteira, South Portugal: Preliminary Results. Geophysical Research Abstracts. Vol. 19, EGU2017-17320, 2017. EGU General Assembly 2017. © Author(s) 2017. CC Attribution 3.0 License.
- Drago T., Silva P., Lopes A., Magalhães V., Roque C., Rodrigues A.I., Noiva J., Terrinha P., Mena A., Francés G., Kopf A., Völker D. & Baptista, M.A. (2016) - Searching for tsunamis evidence on the southern Portuguese continental shelf sedimentary record. European Geosciences Union, General Assembly 2016, Poster in Session EMRP3.4/GI3.11 - Rock magnetism: theory, experiments and observations EGU2016-16997.

Acknowledgments

This research used data (POPEI cores) acquired at the MSCL and XRF Core Scanner Lab at the MARUM – Center for Marine Environmental Sciences, University of Bremen, Germany. We wish to thank to Achim Kopf and David Volker by the kind contribution on the measurements done at MARUM.

The authors wish to acknowledge the R/V Sarmiento de Gamboa crew for their assistance during MOWER cruise, and in particular the chief scientists (Javier Hernández Molina, Gemma Ercilla and David Casas) for the core sampling opportunity.

We also want to thank Guillermo Frances and Anxo Mena by the MSCL and XRF performed on MOWER cores at University of Vigo; Sabine Schmidt from Bordeaux I University for the Pb^{210} analyses and Ana Alberto and Emília Salgueiro for the help with forams preparation and picking for C^{14} analyses.

References

Abrantes, F., Lebreiro, S., Gil, I., Rodrigues, T., Bartels-Jónsdóttir, H., Oliveira, P., Kissel, C., Grimalt, J.O., 2005. Shallow marine sediment cores record climate variability and earthquake activity off Lisbon (Portugal) for the last 2000 years. Quat. Sci. Rev. 24, 2477–2494.

Abrantes F, Alt-Epping U, Lebreiro S et al. (2008) Sedimentological record of tsunamis on shallow-shelf areas: The case of the 1969 AD and 1755 AD tsunamis on the Portuguese Shelf off Lisbon. *Marine Geology* 249: 283–293.

Adams, J., 1990. Paleoseismicity of the Cascadia subduction zone: evidence from turbidites off the Oregon–Washington margin. Tectonics 9, 569–583.

Andrade, C., 1992. Tsunami generated forms in the Algarve barrier islands. Sci.Tsunami Hazards 10, 21–34.

Andrade C, Andrade A, Kortekaas S et al. (1997) Sedimentological traces of tsunamigenic overwash of the Martinhal lowland (Western Algarve – Portugal). *Proceedings Seminário da Zona Costeira do Algarve*. Faro, 10–12 July 1997, Eurocoast-Portugal, pp. 11–18.

Andrade C, Freitas MC, Miranda JM et al. (2003) Recognizing possible tsunami sediments in the ultradissipative environment of the Tagus estuary (Portugal). *Coastal Sediments'03 – The 5th International Symposium on Coastal Engineering and Science of Coastal Sediment Processes*. 18–23 May, Clearwater Beach FL, CD-ROM, 14 pp

Cáceres, L.M., Rodríguez Vidal, J., Ruiz, F., Rodríguez Ramírez, A. and Abad, M., 2006. El registro geológico Holoceno como instrumento para establecer periodos de recurrencia de tsunamis: el caso de la costa de Huelva. *Paper presented at the. V Asamblea Hispano Portuguesa de Geodesia y Geofísica*, Sevilla, pp. 1e4.

Corrochano A, Merino SG, Barba P et al. (2000) Los sedimentos del canal de Mira (Aveiro, Portugal): Propriedades texturales, procedencia y modelo paleogeografico. *Studia Geologica Salmanticensia* 36: 143–160.

Costa, P., Andrade, C., Freitas, M.C., Oliveira, M.A. and Jouanneau, J.M., 2009. Preliminary Results of Exoscopic Analysis of Quartz Grains Deposited by a Palaeotsunami in Salgados Lowland (Algarve, Portugal). *Journal of Coastal Research*, 56, 39-43.

Costa PJM, Andrade C, Freitas MC et al. (2011) Boulder deposition by extreme marine events. *Earth Surface Processes and Landforms* DOI: 10.1002/ esp.2228.

Craft C.B., Seneca E.D. and Broome S.W, 1991, Loss on Ignition and Kjeldahl Digestion for Estimating Organic Carbon and Total Nitrogen in Estuarine Marsh Soils: - Calibration with Dry Combustion. Estuaries Vol. 14, No. 2, pp. 175-179

Dabrio, Cj., Goy, j.L, law, C, 1999. The record of the tsunami produced by the 1755 Lisbon earthquake in Valdelagrana spit (Gulf of Cadiz, southern Spain). Geogaceta 23, 31-34.

Dawson, A.G., Hindson, R.A., Andrade, C., Freitas, C., Parish, R., Bateman, M. 1995. Tsunami sedimentation associated with the Lisbon earthquake of 1 November AD1755: Boca do Rio, Algarve, Portugal.Holocene 5 (2), 209–215.

Dawson, A.G., Stewart, I., 2007. Tsunami deposits in the geological record. Sediment. Geol. 220 (3–4), 166–183. doi:10.1016/j.sedgeo.2007.01.002.

Dekkers, M.J., 1988. Magnetic properties of natural pyrrholte Part I: Behaviour of initial susceptibility and saturation-magnetization-related rock-magnetic parameters in a grain-size dependet framework. PEPI 52, 376-393.

Dunlop, D. J., and Ö. Özdemir (1997), Rock Magnetism, Fundamentals and Frontiers, Cambridge Univ. Press, Cambridge, U. K., doi:10.1017/CBO9780511612794.

Evans, M.E. and Heller, F., 2003. Environmental Magnetism – Principles and Applications of Enviromagnetics. Academic Press, 299pp.

Font, E., Nascimento, C., Omira, R., Baptista, M.A., Silva, P.F., 2010. Identification of tsunami-induced deposits using numerical modeling and rock magnetism techniques: A study case of the 1755 Lisbon tsunami in Algarve, Portugal. *Physics of the Earth and Planetary Interiors*, 182, 187–198. doi:10.1016/j.pepi.2010.08.007

Garcia-Orellana, J., Gràcia, E., Vizcaino, A., Masqué, P., Olid, C., Martinez- Ruiz, F., Piñero, H., Sanchez-Cabeza, J.-A., Dañobeitia, J., 2006. Identifying instrumental and historical earthquake records in the SW Iberian margin using 210Pb turbidite chronology. Geophys. Res. Lett. 33, L24601.doi:10.1029/2006GL028417.

Goldfinger, C., Nelson, C.H., Johnson, J.E., Shipboard Scientific Party, 2003. Holocene earthquake records from the Cascadia subduction zone and northern San Andreas Fault based on precise dating of offshore turbidites. Annual Reviews of Earth and Planetary Science 31, 555–577.

Hindson, R.A., Andrade, C., Dawson, A.G., 1996. Sedimentary processes associated with the tsunami generated by the 1755 Lisbon earthquake on the Algarve coast, Portugal. Phys. Chem. Earth 21, 57–63.

Hindson, R.A. and C. Andrade, 1999. Sedimentation and hydrodynamic processes associated with the Tsunami generated by the 1755 Lisbon earthquake, Quaternary International, 56, 27-38.

Hrouda, F. , Chlupáčová M., Pokorný J., 2006, Low-field variation of magnetic susceptibility measured by the KLY-4S Kappabridge and KLF-4A magnetic susceptibility meter: Accuracy and interpretational programme. Studia Geophysica et Geodaetica, 50, 2, 283–299

Kortekaas S and Dawson AG (2007) Distinguishing tsunami and storm deposits: An example from Martinhal, SW Portugal. *Sedimentary Geology* 200(3–4): 208–221.

Lario, j., 1996. Ultimo y Presente Interglacial en el area de conexion Atlantico - Mediterraneo: Variaciones del nivel del mar, palaeoclima y palaeoambientes. Ph.D. thesis. Universidad Complutense de Madrid, p. 269.

Lario, J., law, C, Dabrio, CJ., Somoza, L, Goy, j.L, Bardaji, T., Silva, P.G., 1995. Record of recent Holocene sediment Input on spit bars and Deltas of south Spain. In: Core, B. (Ed.), Holocene Cycles: Climate, Sea Levels, and Sedimentation. Journal of Coastal Research, 17, pp. 241-245.

Lebreiro, S.M., McCave, I.N., Weaver, P.P.E., 1997. Late Quaternary turbidite emplacement on the Horseshoe Abyssal Plain (Iberian Margin). Journal of Sedimentary Research 67 (5), 856–870.

Liu, Q., A. P. Roberts, J. C. Larrasoaña, S. K. Banerjee, Y. Guyodo, L. Tauxe, and F. Oldfield (2012), Environmental magnetism: Principles and applications, Rev. Geophys., 50, RG4002, doi:10.1029/2012RG000393.

Lowrie, W., and Heller, F., 1982, Magnetic properties of marine limestones, *Rev. Geophys*., 20, 171-192.

Luque, L, Lario,j., law, C, Goy, j.L, Dabrio, Cj., Silva, P.G., 2001. Tsunami deposits as palaeoseismic indicators: examples from the Spanish coast. Acta Geologica Hispanica 36, 197-211.

Luque, L, Lario, J., law, C, Goy, j.L, Dabrio, Cj., Borja, E, 2002. Sedimentary record of historical tsunamis in the Bay ofCadiz (Spain). Journal of Quaternary Science 17,623-631.

Mil-Homens Mário, Vale C., Naughton F, Brito P., Drago T., Anesa B., Raimundo J., Schmidt S. and Caetano M. (2016) - Footprint of roman and modern mining activities in a sediment core from the southwestern Iberian Atlantic shelf. Science of The Total Environment, Volume 571, 15 November 2016, Pages 1211–1221.

Morales, J.A., Borrego, J., San Miguel, E.G., López-González, N., Carro, B., 2008. Sedimentary record of recent tsunamis in the Huelva Estuary (southwestern Spain). Quaternary Science Reviews 27, 734e746.

Mitra, R., Tauxe, L., 2009. Full vector model for magnetization in sediments. EPSL 286, 535-545.

Omira, R., Ramalho, I., Terrinha, P., Baptista, M.A., Batista, L., Zitellini, N., 2016. Deep-water seamounts, a potential source of tsunami generated by landslides? The Hirondelle Seamount, NE Atlantic. Marine Geology 379, 267-280.

Ozdemir, O., Dunlop, D.J., Berquo, T.S., 2008. Morin transition in hematite: Size dependence and thermal hysteresis. Geochem Geophy Geosy 9

Quintela M., Costa P.J.M., Fatela F., Drago T., Hoska N., Andrade C. & Freitas M.C. (2016) -The AD 1755 tsunami deposits onshore and offshore of Algarve (south Portugal): Sediment transport interpretations based on the study of Foraminifera assemblages. Quaternary International, 408-A, 123-138.

Reicherter, K, Vonberg, D., Koster, B., Fernandez-Steeger, T., Griltzner, C, MathesSchmidt, M., 2010. The sedimentary inventory of tsunamis along the southern Gulf of Cadiz (southwestern Spain). leitschrift fUr Geomorphologie 54 (Supp1.3),147-173

Ruiz, E, Borrego, j., L6pez-Gonzalez, N., Abad, M., Gonzalez-Regalado, M.L, Carro, B., Pendon, j.G., Rodriguez Vidal, j., Caceres, LM., Prudencio, M.I., Dias, M.I., 2007. The geological record of a mid-Holocene marine storm in southwestern Spain. Geobios 40 689-669.

Ruiz, E, Rodriguez Ramirez, A, Caceres, L, Rodriguez Vidal, j., Carretero, M.I., Abad, M., Olias, M., Pow, M., 2005. Evidence of high-energy events in the geological records: mid-Holocene evolution of the southwestern Donana national park (SW Spain). Paleogeography, Paleoc1imatology, Paleoecology 229, 212-229.

Ruiz, E, Rodriguez Ramirez, A, Caceres, L, Rodriguez Vidal, j., Carretero, M.I., Clemente, L, Munoz, j.M., Yanez, C, Abad, M., 2004. Late Holocene evolution of the southwestern DonanaNacional Park (Guadalquivir estuary, SW Spain): a multivariate approach. Paleogeography, Paleoc1imatology, Paleoecology 204, 47-64.

Scheffers A and Kelletat D (2005) Tsunami relics on the coastal landscape west of Lisbon, Portugal. *Science of Tsunami Hazards* 23(1): 3–16.

Schneider H, Höfer D, Trog C et al. (2009) Holocene estuary development in the Algarve Region (Southern Portugal) – A reconstruction of sedimentological and ecological evolution. *Quaternary International* 221(1–2): 141–158.

Shanmugam, G., 2006. The tsunamite problem: *J. Sed. Res*., 76, 718-730.

Shiki, T. and T. Yamazaki, 1996. Tsunami-induced conglomerates in Miocene upper bathyal deposits, ChitaPeninsula, central Japan; Marine sedimentary events and their records: *Sed. Geol*., 104, 175-188.

Silva, PF., Drago, T., Guerreiro, C, Caetano, M., Oliveira A. Duarte J.F., Naugthon, F. And Gomes, S (2012) - Magnetic variability along the Holocene sedimentary record in the southern Portuguese continental shelf. Proceedings of MIA2012, p.57, Lisboa.

Tatzber M, Stemmer M, Spiegel H, Katzlberger C, Haberhauer G, Gerzabek (2007) - An alternative method to measure carbonate in soils by FT-IR spectroscopy. Environ Chem Lett.;5:9–12. doi: 10.1007/s10311-006-0079-5.

Thomson, J., Weaver, P.P.E., 1994. An AMS radiocarbon method to determine the emplacement time of recent deep-sea turbidites. Sedimentary Geology 89, 1-7.

Whelan, E, Kelletat, D., 2005. Boulder deposits on the southern Spanish Atlantic coast: possible evidence for the 1755 AD Lisbon tsunami? The Science of Tsunami Hazards 23, 25-38.
Vizcaino, A., Gracia, E., Pallas, R., Garcia-Orellana, J., Escutia, C., Casas, D., Willmott, V., Diez, S., Asioli, A., Danobeitia, J.J., 2006. Sedimentology, physical properties and ages of mass-transport deposits associated to the Marqueˆs de Pombal Fault, Southwest Portuguese Margin. Norwegian Journal of Geology 86, 177–186.